Electronic Supplementary Material (ESI) for Inorganic Chemistry Frontiers.
This journal is © the Partner Organisations 2016

Supplementary Information

Six- and seven-coordinate Fe(II) and Zn(II) compounds ligated by unsymmetric xanthene-based ligands: characterization and magnetic properties

Ruth M. Haas,[a] Muhammad Arshad,[b,‡] James Anthony,[b] Philipp J. Altmann,[a] Alexander Pöthig,[a] Frank H. Köhler [a] and Corinna R. Hess[a,*]

[a.] Technische Universität München, Department of Chemistry and Catalysis Research Center, Lichtenbergstraße 4, 85748 Garching, Germany.

[b.] Durham University, Department of Chemistry, South Road, Durham, DH1 3LE, UK.

‡ current address: Institute of Chemistry, University of the Punjab, Quaid-i-Azam Campus, Lahore-54590, Pakistan.

*Email: corinna.hess@ch.tum.de

Figure S1. ^{1}H NMR (400 MHz, $CDCl_3$) spectrum of *tert*-butyl (5-amino-2,7-di-*tert*-butyl-9,9-dimethyl-xanthen-4-yl)carbamate (**1**).

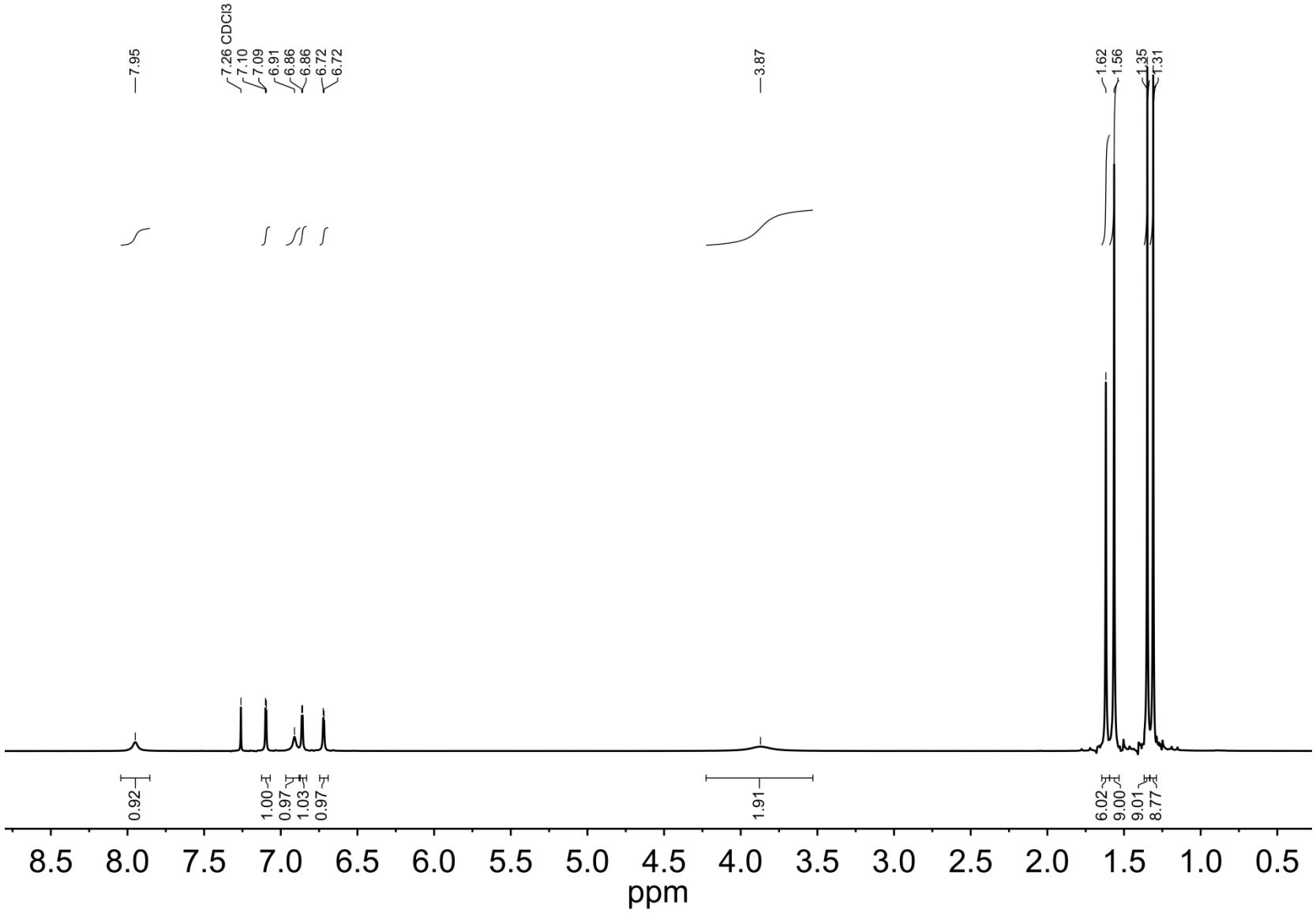

Figure S2. ^{13}C NMR (100 MHz, $CDCl_3$) spectrum of *tert*-butyl (5-amino-2,7-di-*tert*-butyl-9,9-dimethyl-xanthen-4-yl)carbamate (**1**).

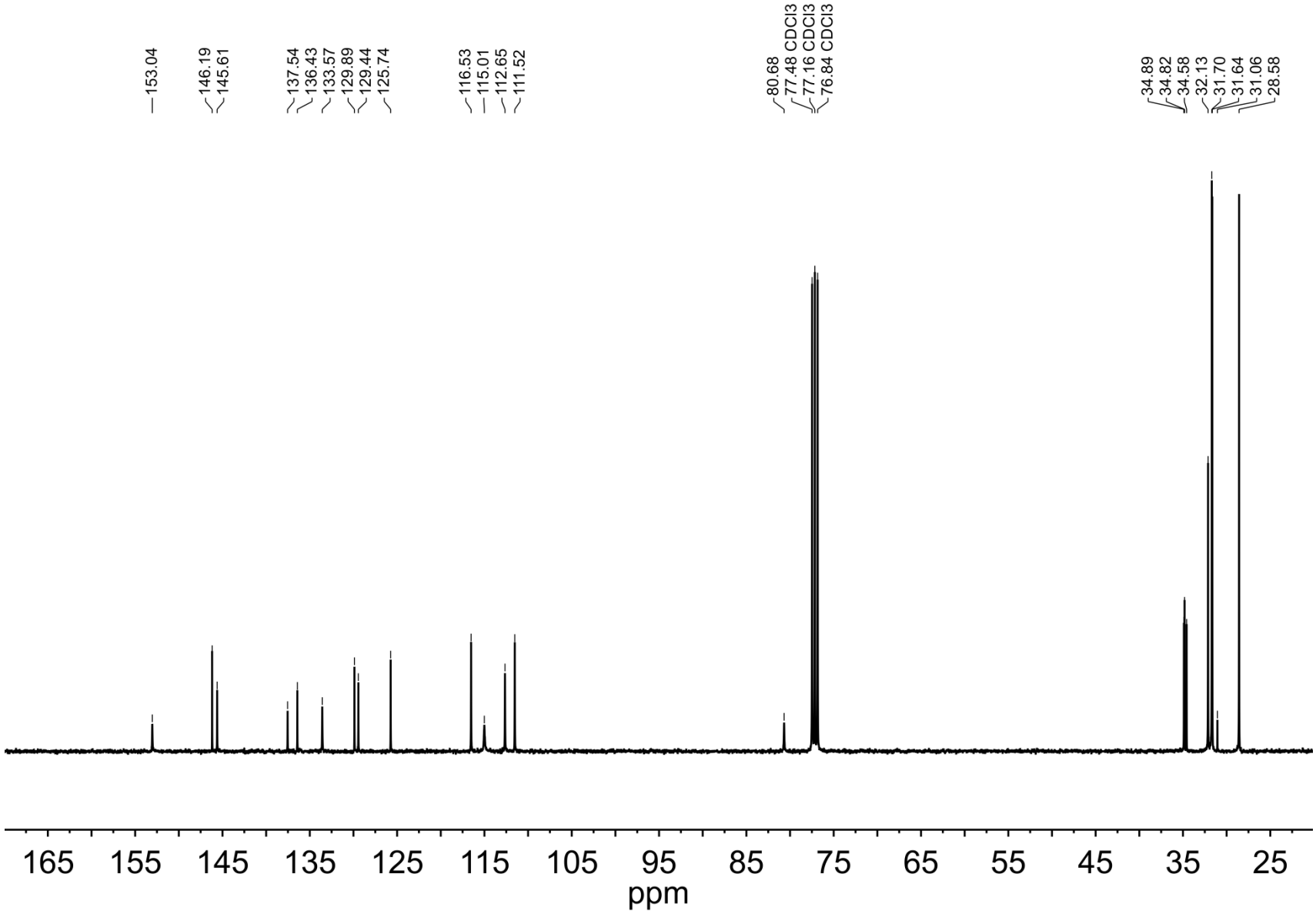

Figure S3. ^{1}H NMR (400 MHz, $CDCl_3$) spectrum of *tert*-butyl (2,7-di-*tert*-butyl-9,9-dimethyl-5-((pyridin-2-ylmethyl)amino)-xanthen-4-yl)carbamate (**2a**).

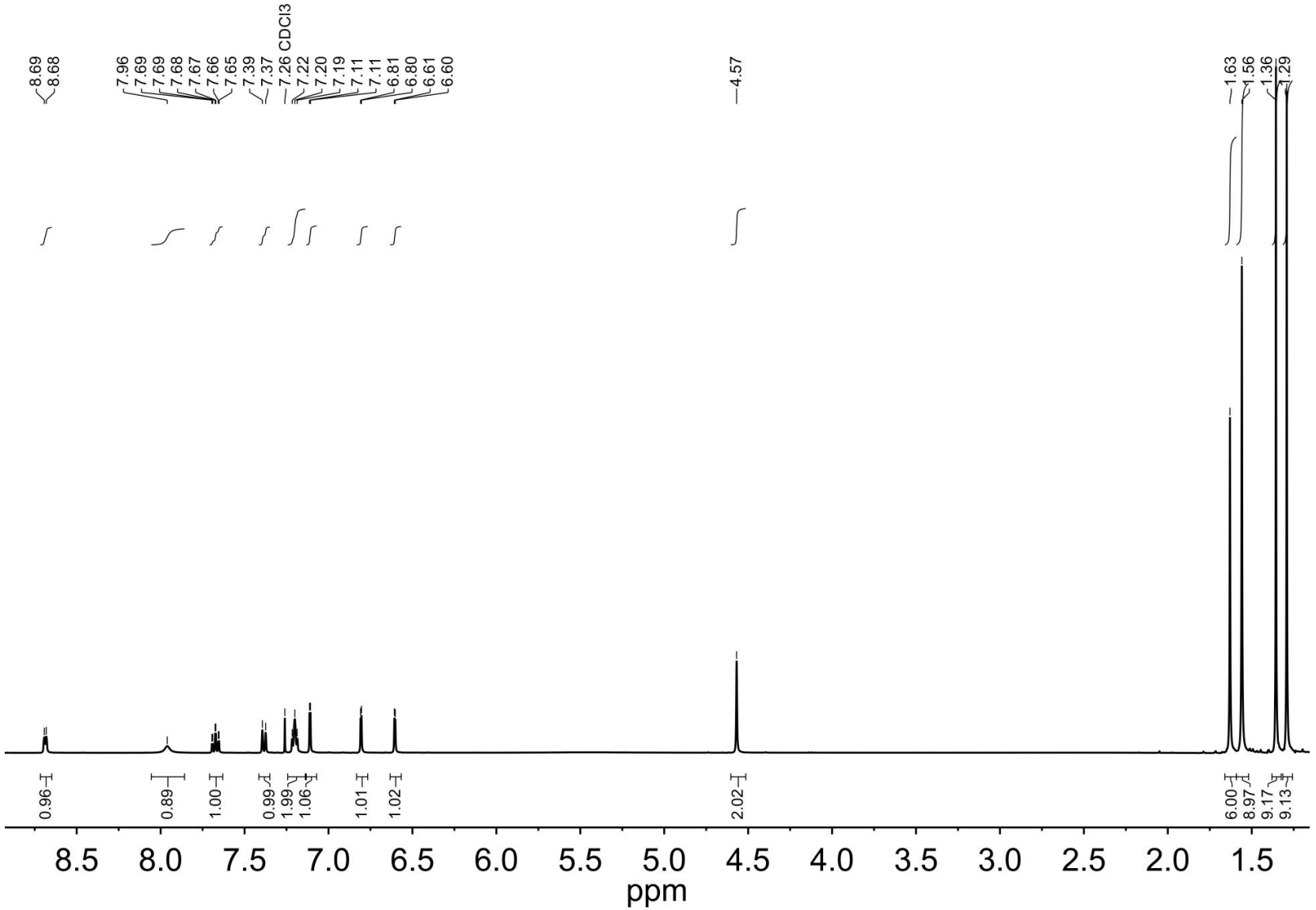

Figure S4. ^{13}C NMR (100 MHz, $CDCl_3$) spectrum of *tert*-butyl (2,7-di-*tert*-butyl-9,9-dimethyl-5-((pyridin-2-ylmethyl)amino)-xanthen-4-yl)carbamate (**2a**).

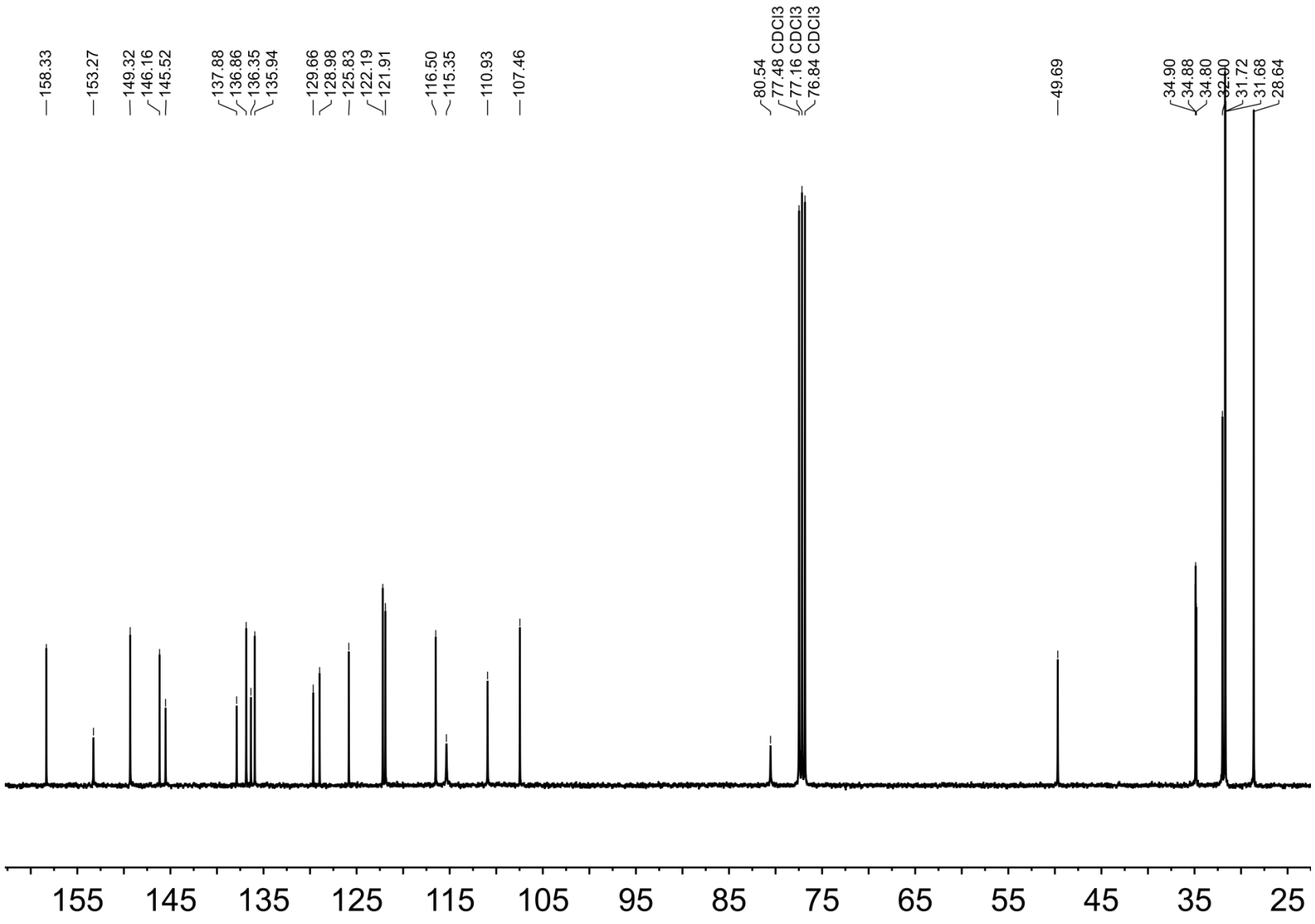

Figure S5. ^{1}H NMR (400 MHz, $CDCl_3$) spectrum of *tert*-butyl (5-(bis(pyridin-2-ylmethyl)amino)-2,7-di-*tert*-butyl-9,9-dimethyl-xanthen-4-yl)carbamate (**2b**).

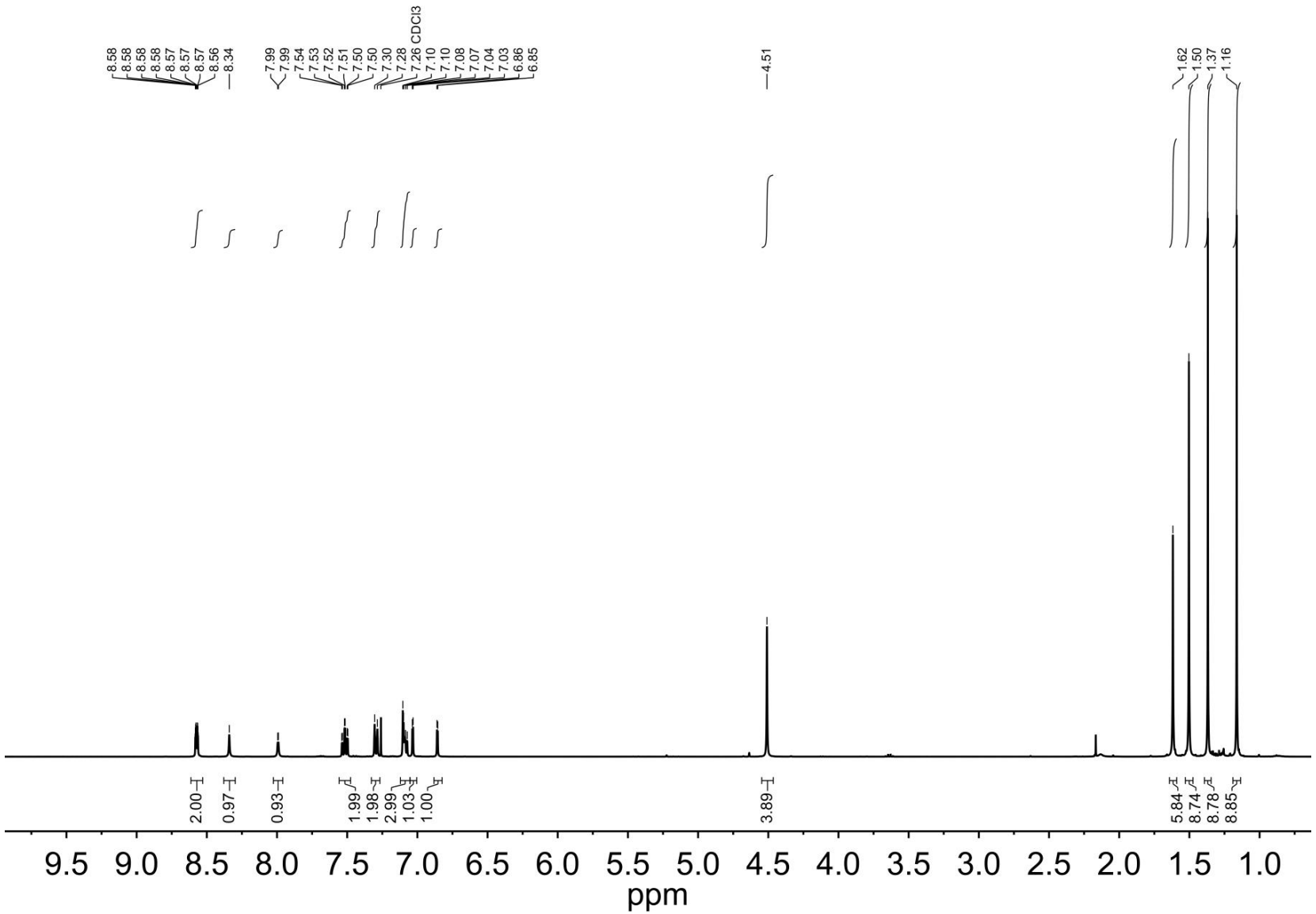

Figure S6. ^{13}C NMR (100 MHz, $CDCl_3$) spectrum of *tert*-butyl (5-(bis(pyridin-2-ylmethyl)amino)-2,7-di-*tert*-butyl-9,9-dimethyl-xanthen-4-yl)carbamate (**2b**).

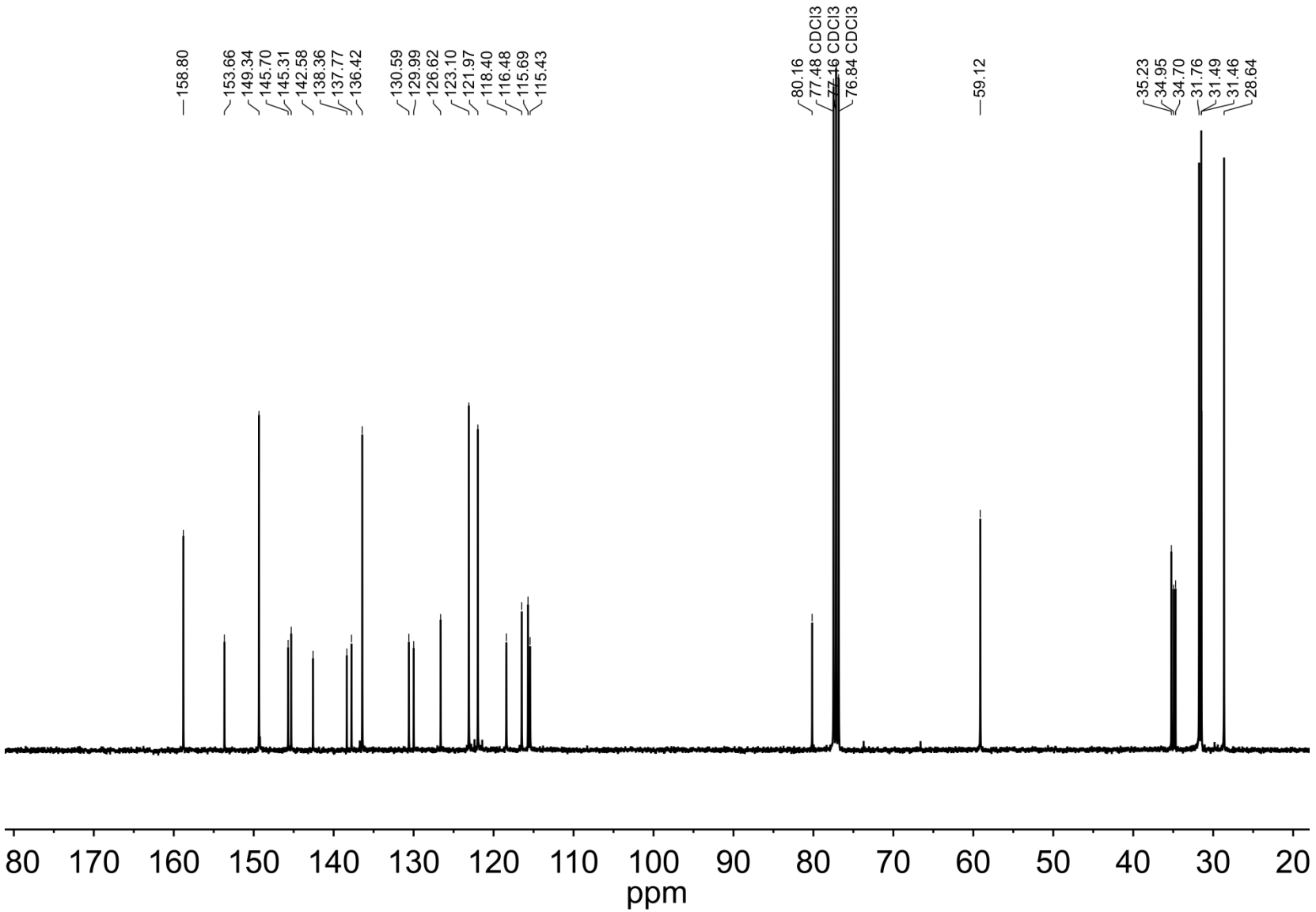

Figure S7. ^{1}H NMR (400 MHz, $CDCl_3$) spectrum of 2,7-di-*tert*-butyl-9,9-dimethyl-N-(pyridin-2-ylmethyl)-xanthene-4,5-diamine (**3a**).

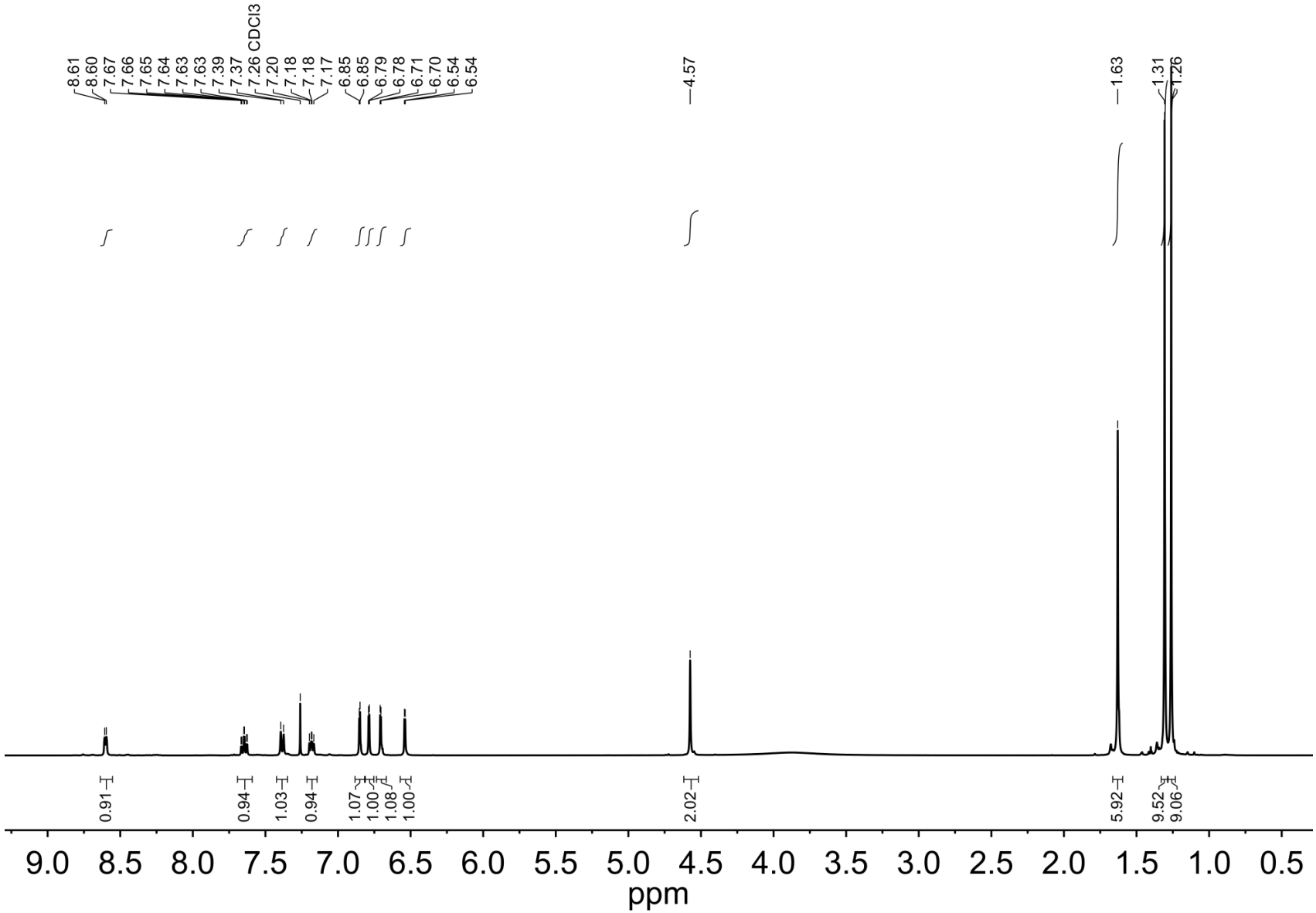

Figure S8. ^{13}C NMR (100 MHz, $CDCl_3$) spectrum of 2,7-di-*tert*-butyl-9,9-dimethyl-N-(pyridin-2-ylmethyl)-xanthene-4,5-diamine (**3a**).

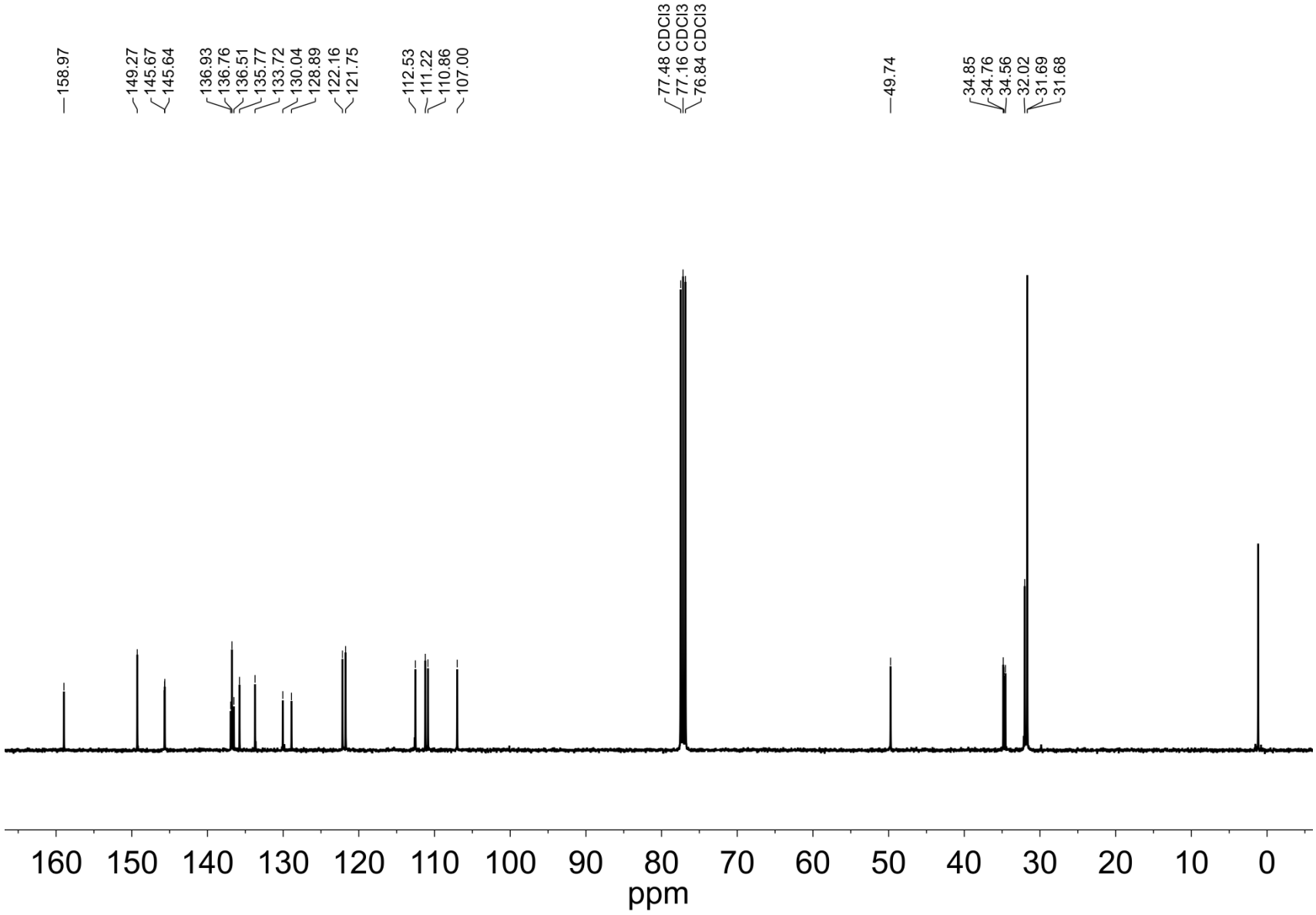

Figure S9. ^{1}H NMR (400 MHz, $CDCl_3$) spectrum of 2,7-di-*tert*-butyl-9,9-dimethyl-N,N-bis(pyridin-2-ylmethyl)-xanthene-4,5-diamine (**3b**).

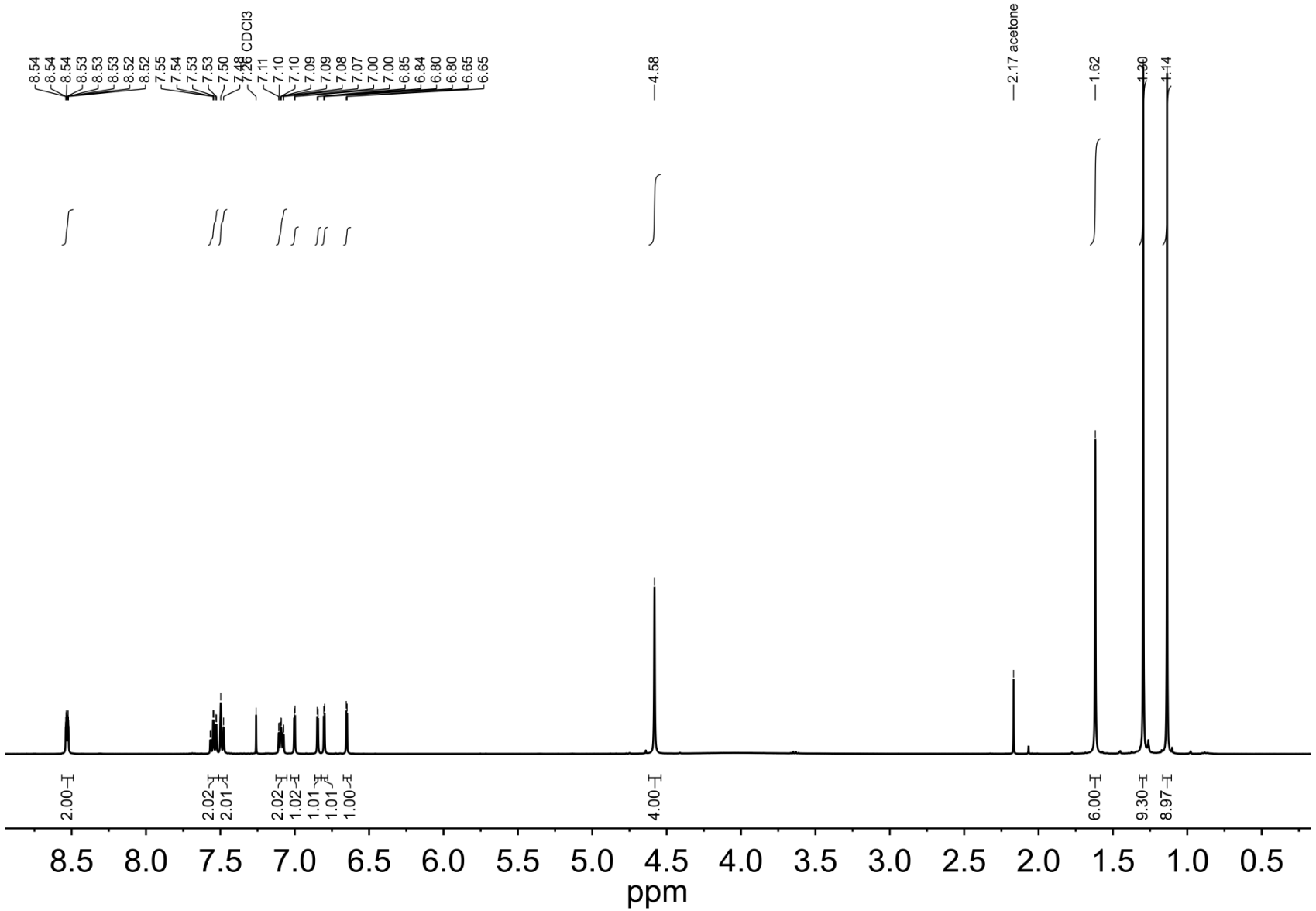

Figure S10. ^{13}C NMR (100 MHz, $CDCl_3$) spectrum of 2,7-di-*tert*-butyl-9,9-dimethyl-N,N-bis(pyridin-2-ylmethyl)-xanthene-4,5-diamine (**3b**).

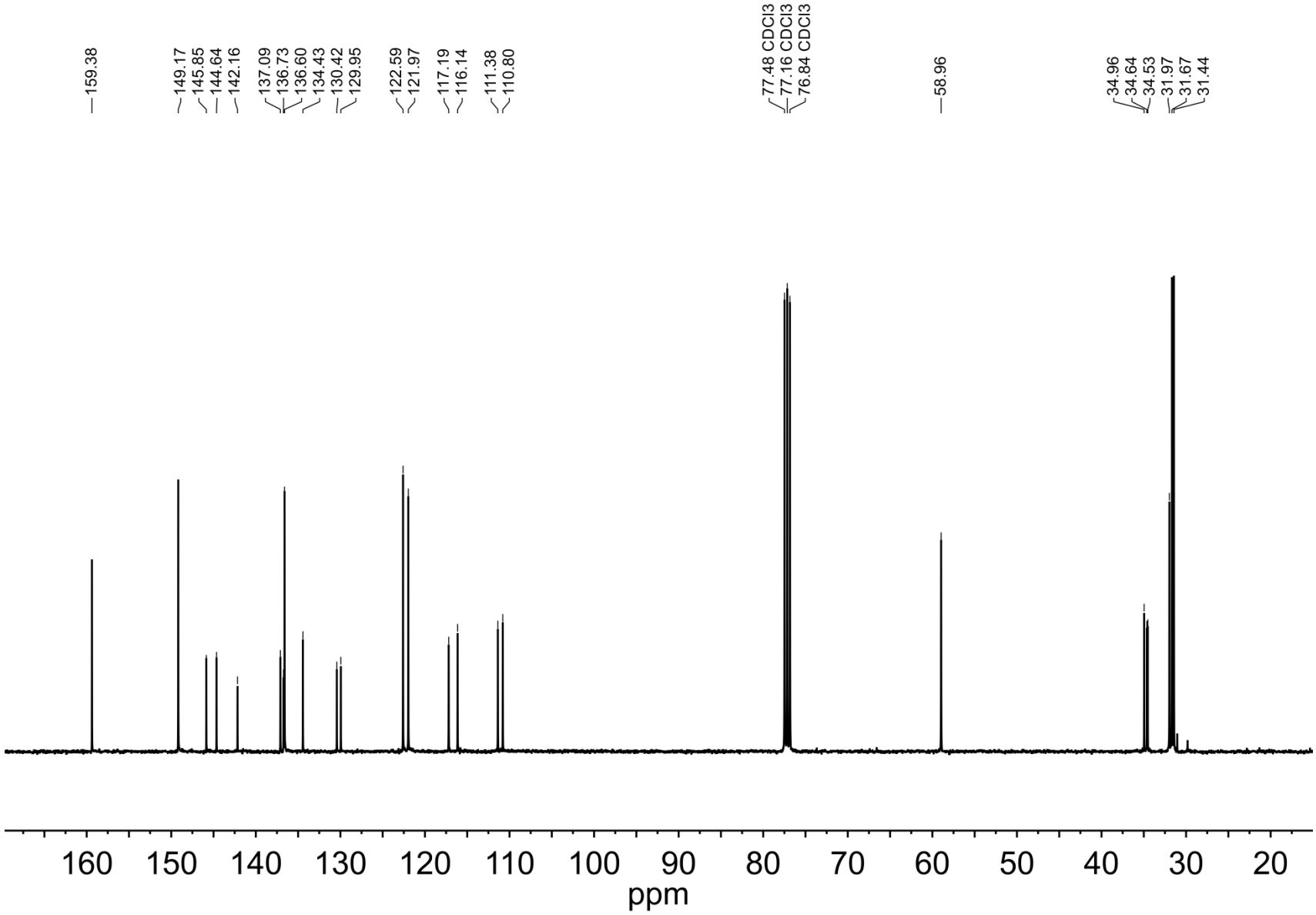

Figure S11. ^{1}H NMR (600 MHz, $CDCl_3$) spectrum of **iXa**.

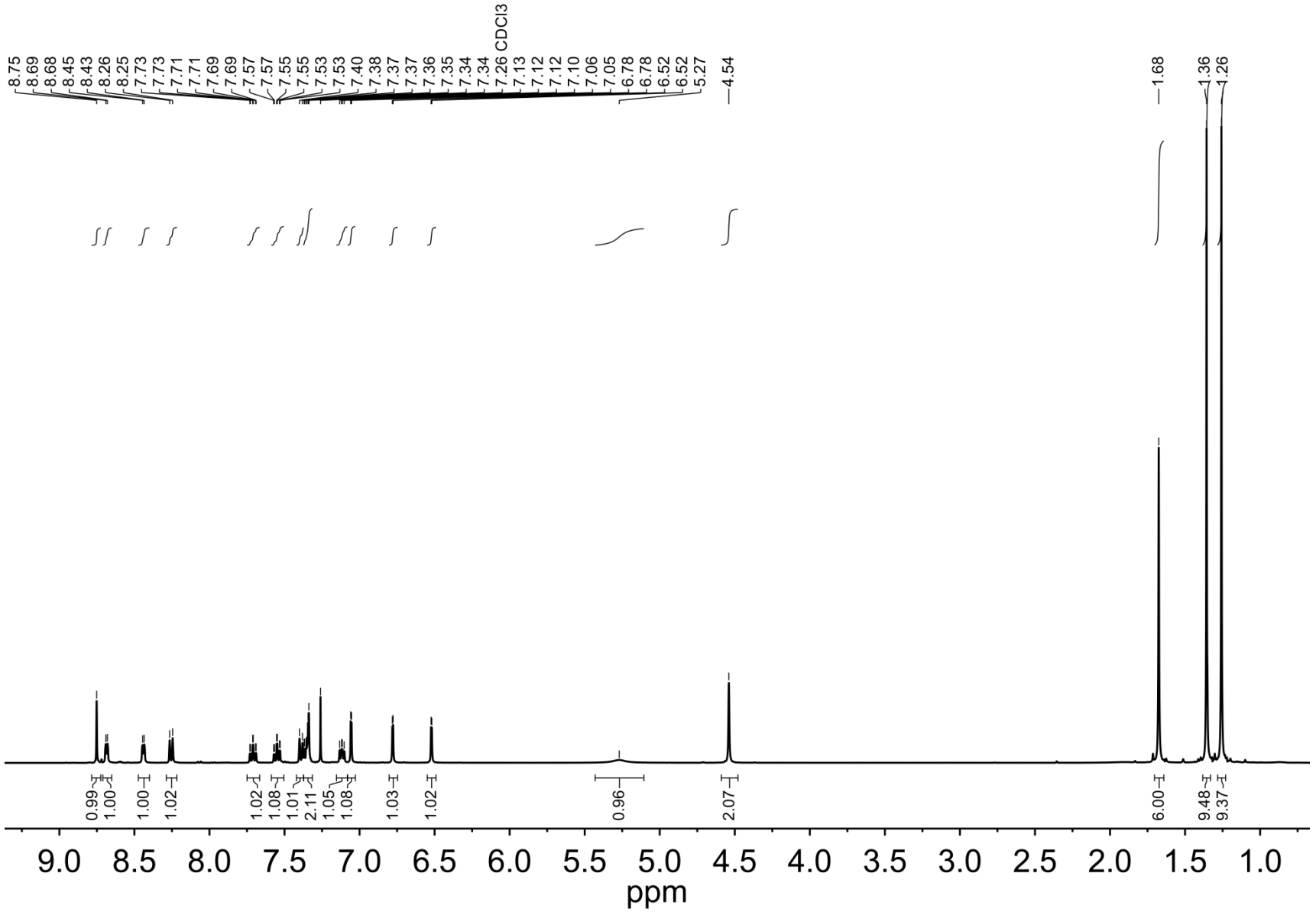

Figure S12. ^{13}C NMR (151 MHz, $CDCl_3$) spectrum of **iXa**.

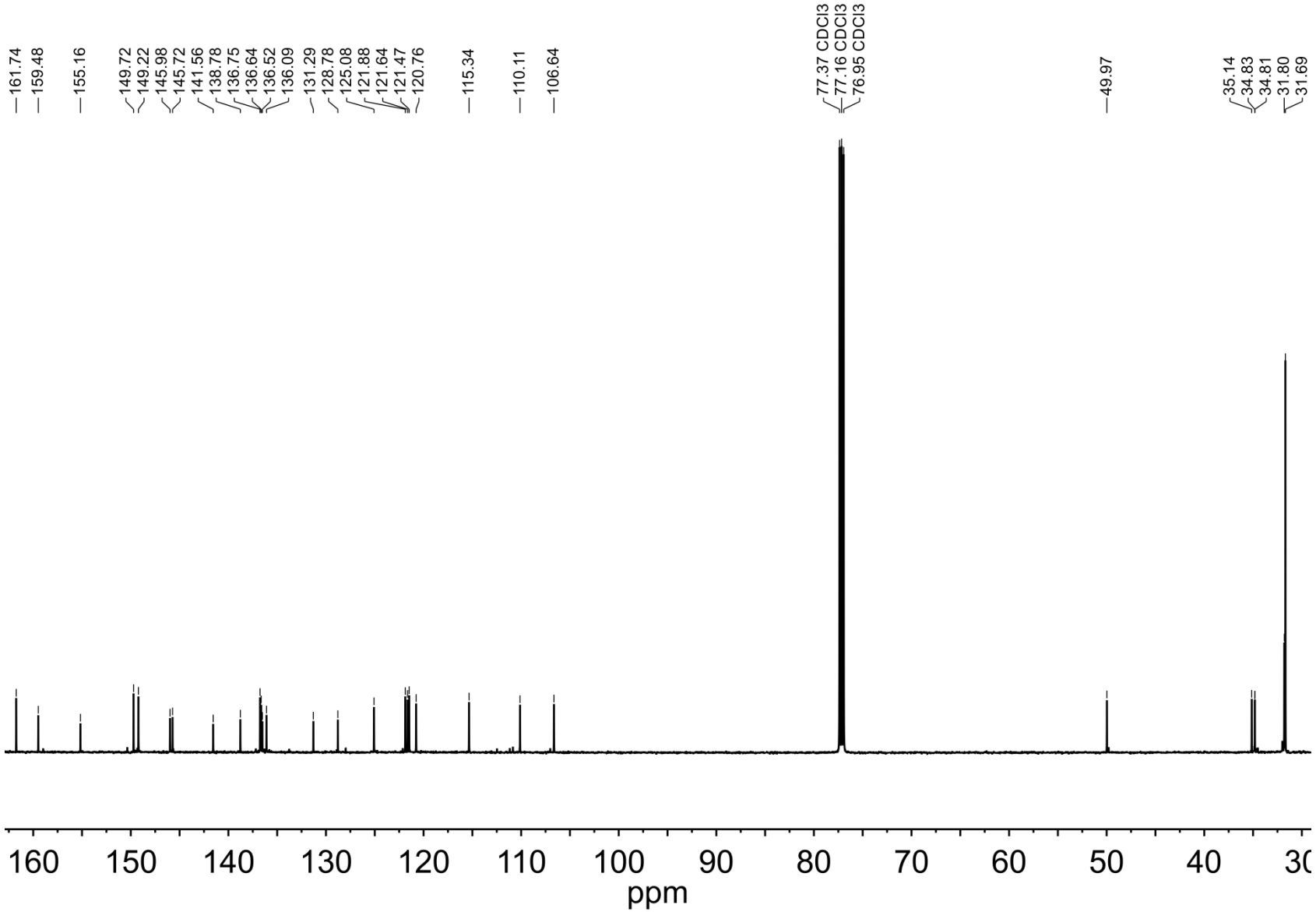

Figure S13. ^{1}H cosy-NMR spectrum (600 MHz, $CDCl_3$) spectrum of **iXa**.

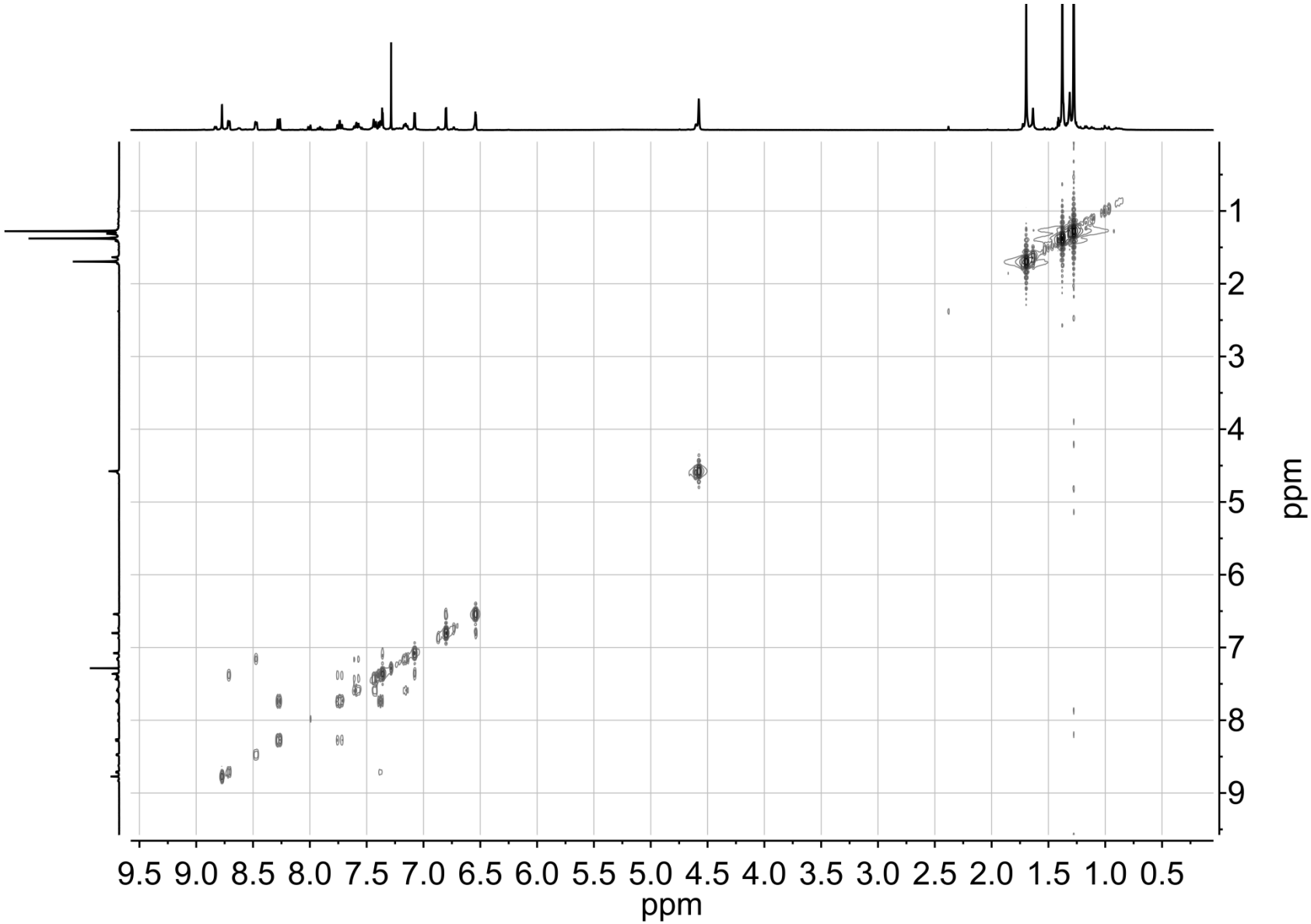

Figure S14. ^{1}H, ^{13}C HSQC-NMR spectrum (600 MHz, 151 MHz, $CDCl_3$) spectrum of **iXa**.

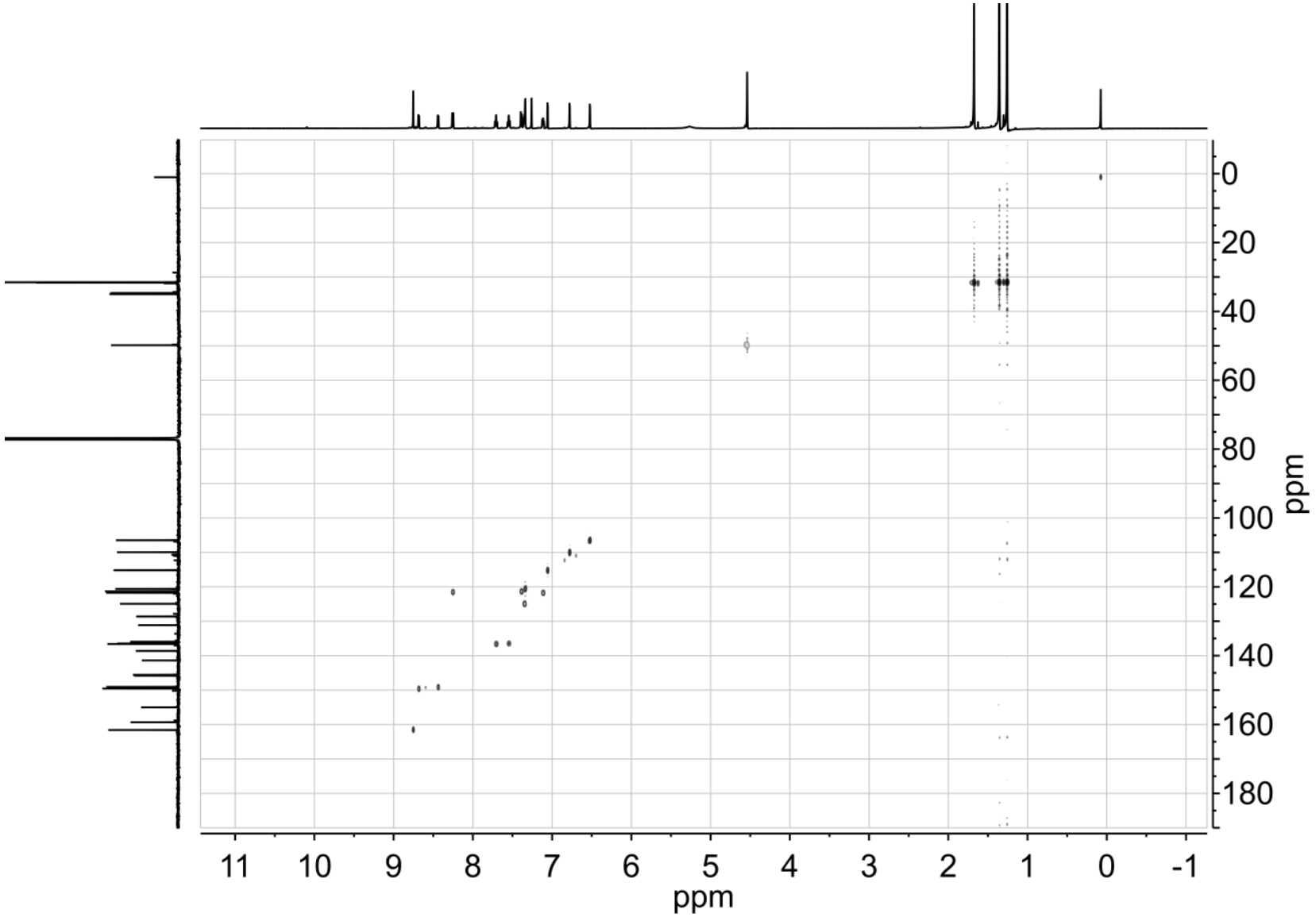

Figure S15. ^{1}H, ^{13}C HMBC-NMR spectrum (600 MHz, 151 MHz, $CDCl_3$) spectrum of **iXa**.

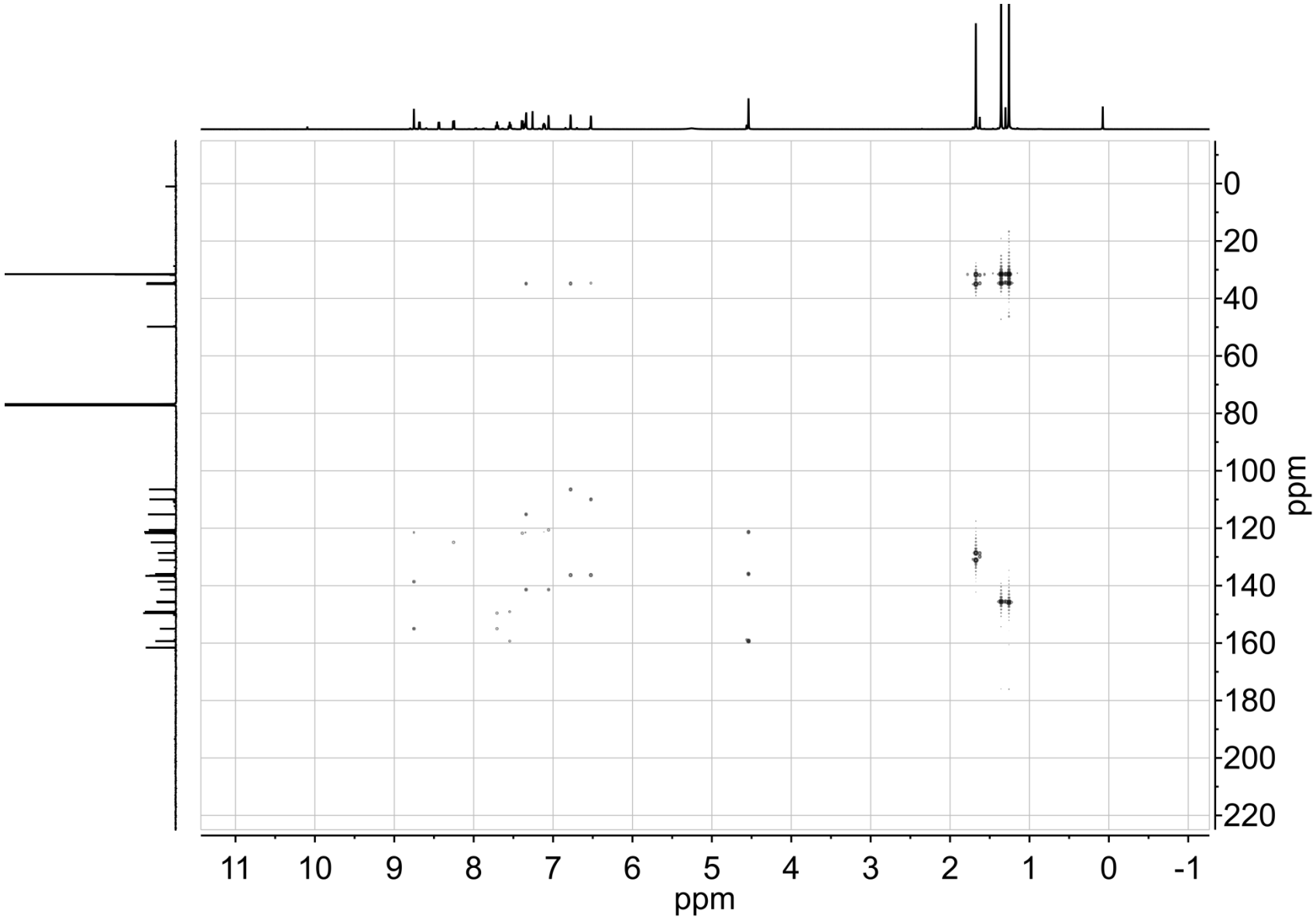

Figure S16. ^{1}H NMR (600 MHz, $CDCl_3$) spectrum of **iXa-2**.

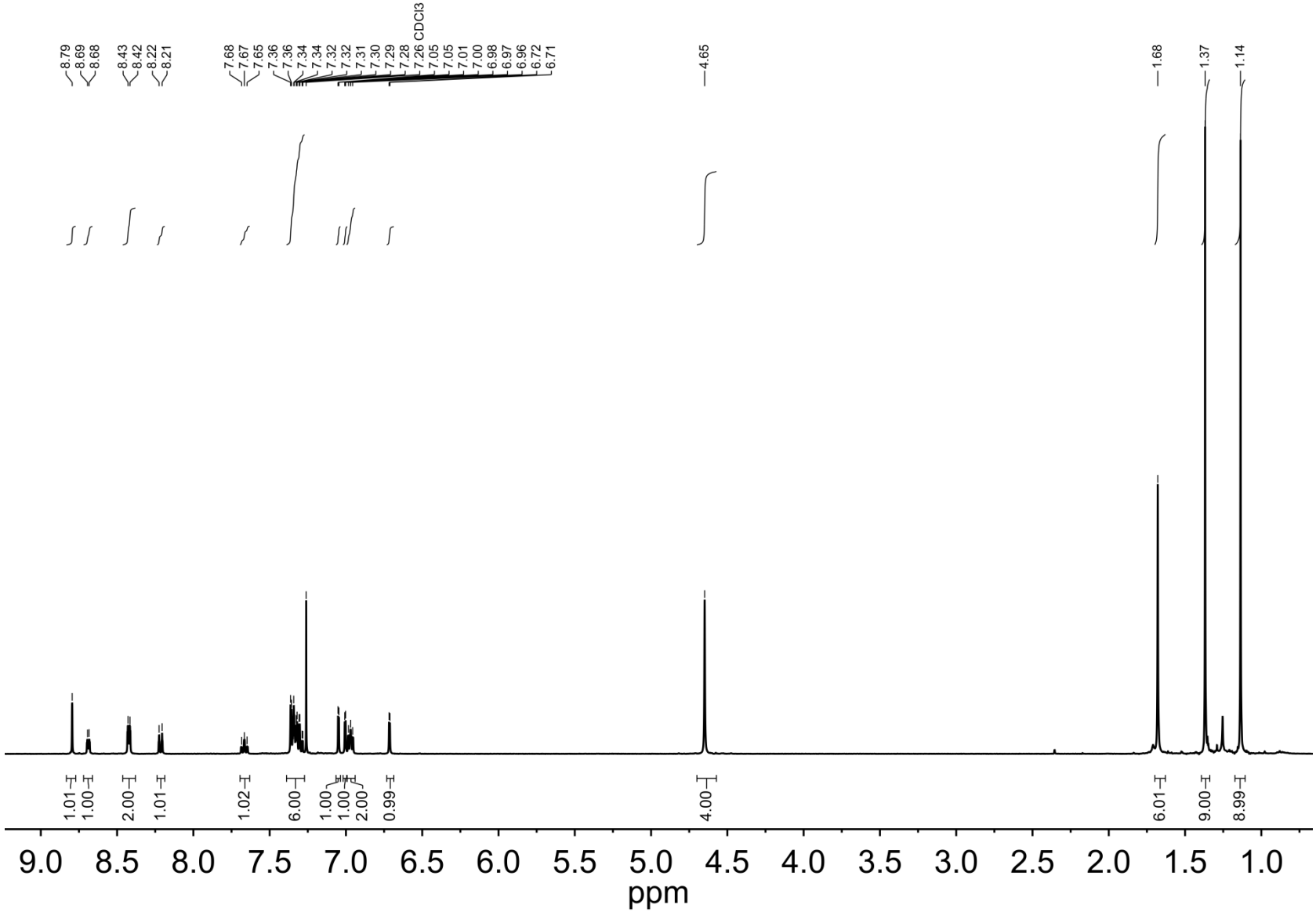

Figure S17. ^{13}C NMR (151 MHz, $CDCl_3$) spectrum of **iXa-2**.

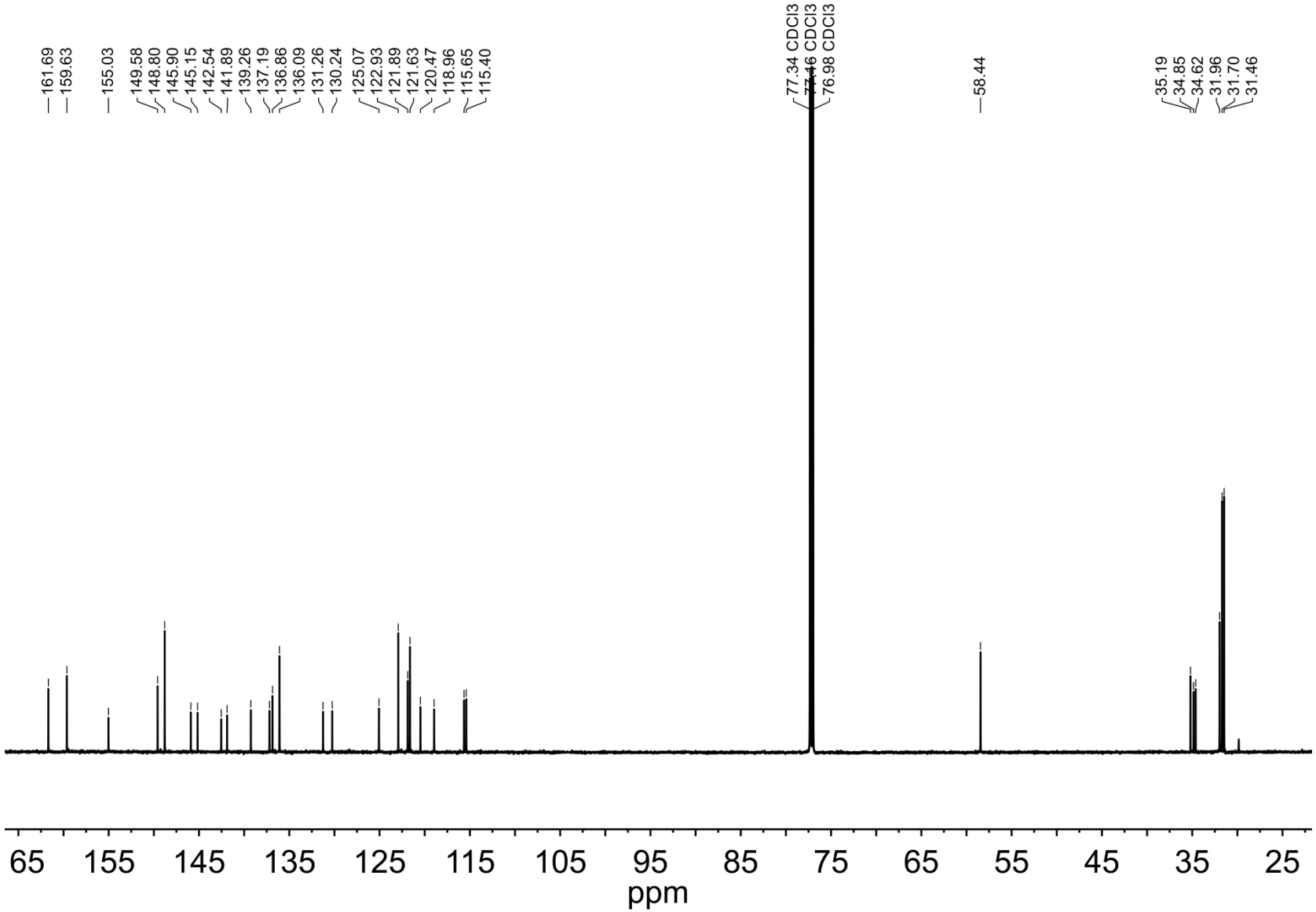

Figure S18. ^{1}H cosy-NMR spectrum (600 MHz, $CDCl_3$) spectrum of **iXa-2**.

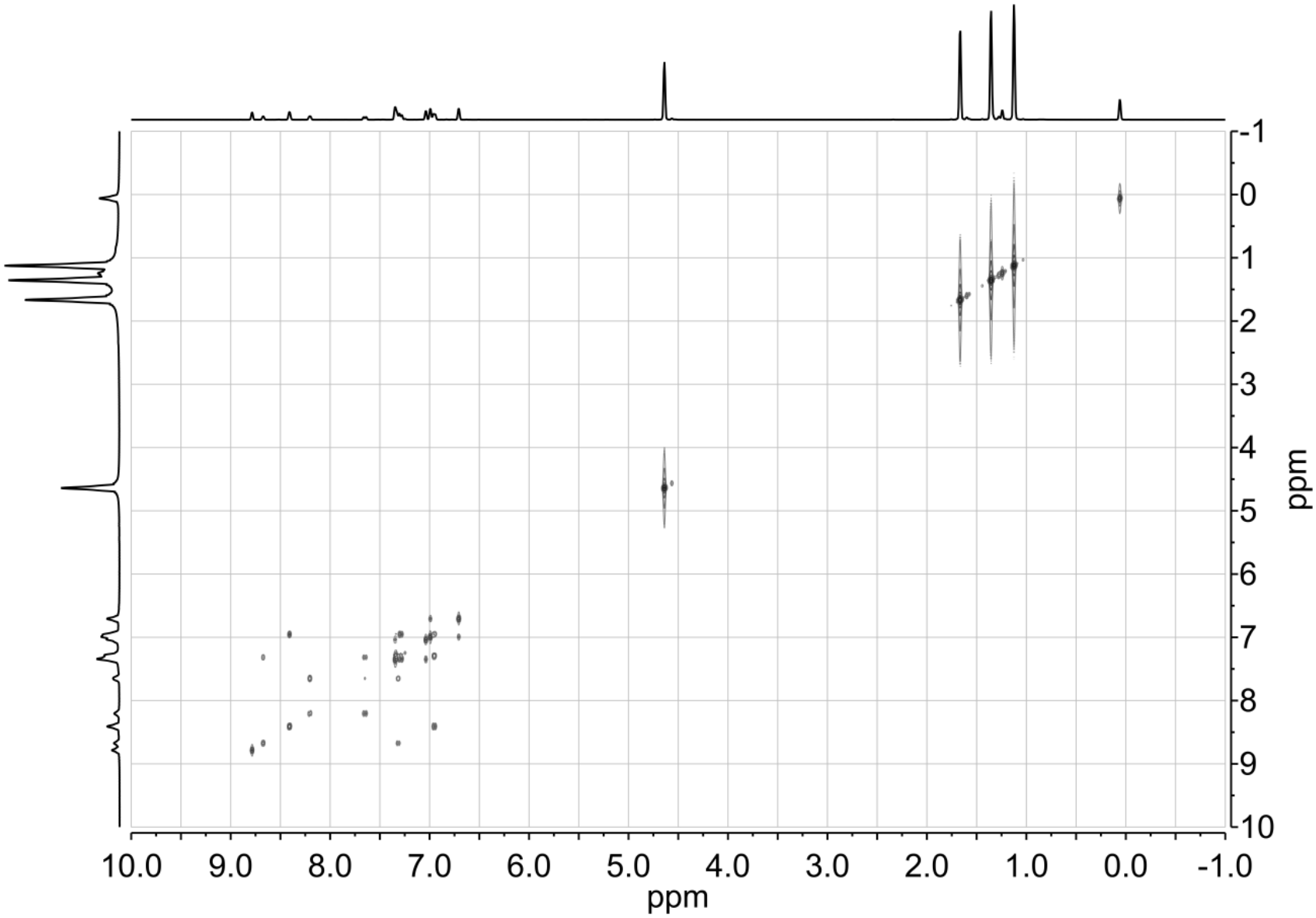

Figure S19. ^{1}H, ^{13}C HSQC-NMR spectrum (600 MHz, 151 MHz, $CDCl_3$) spectrum of **iXa-2**.

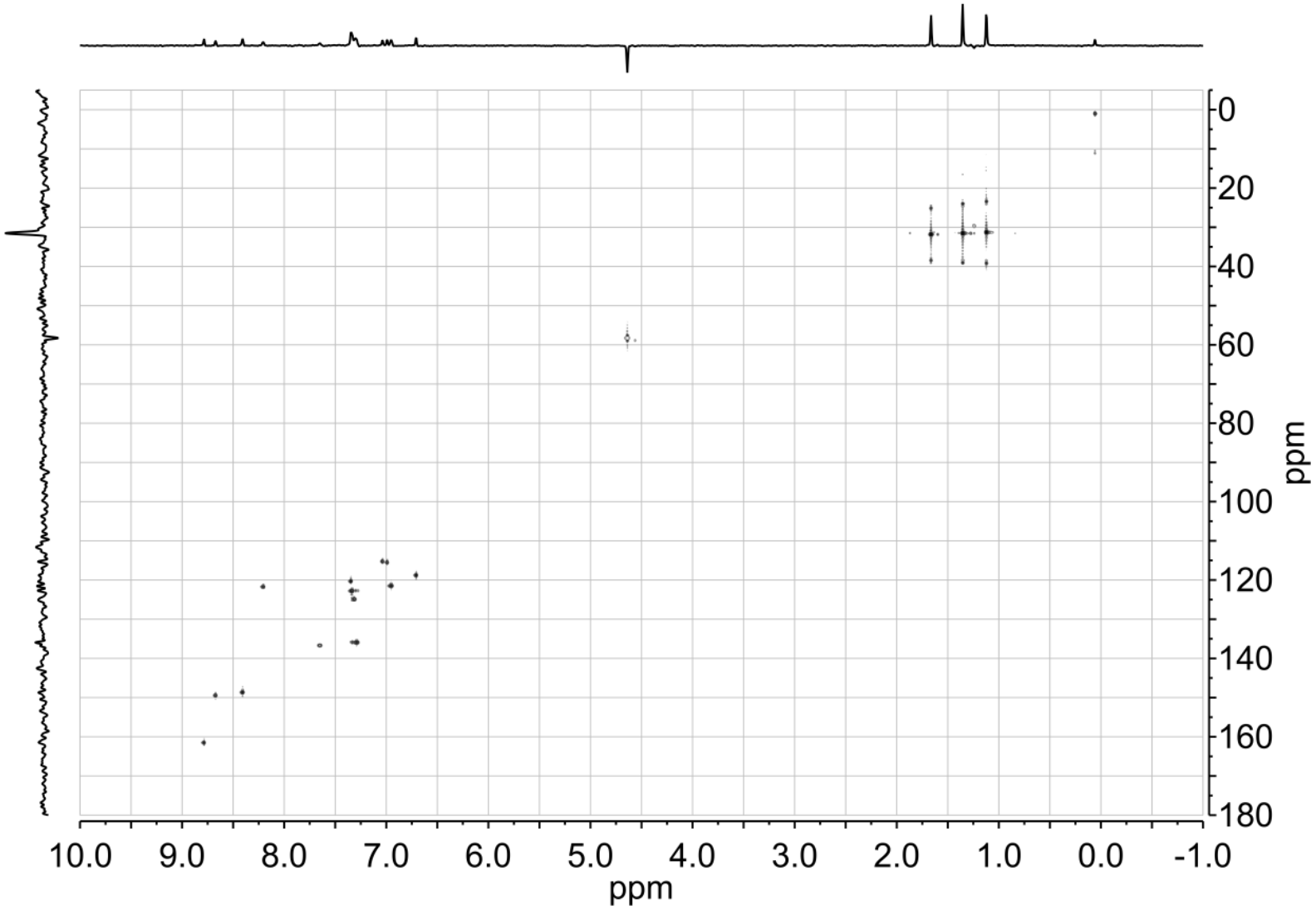

Figure S20. ^{1}H, ^{13}C HMBC-NMR spectrum (600 MHz, 151 MHz, $CDCl_3$) spectrum of **iXa-2**.

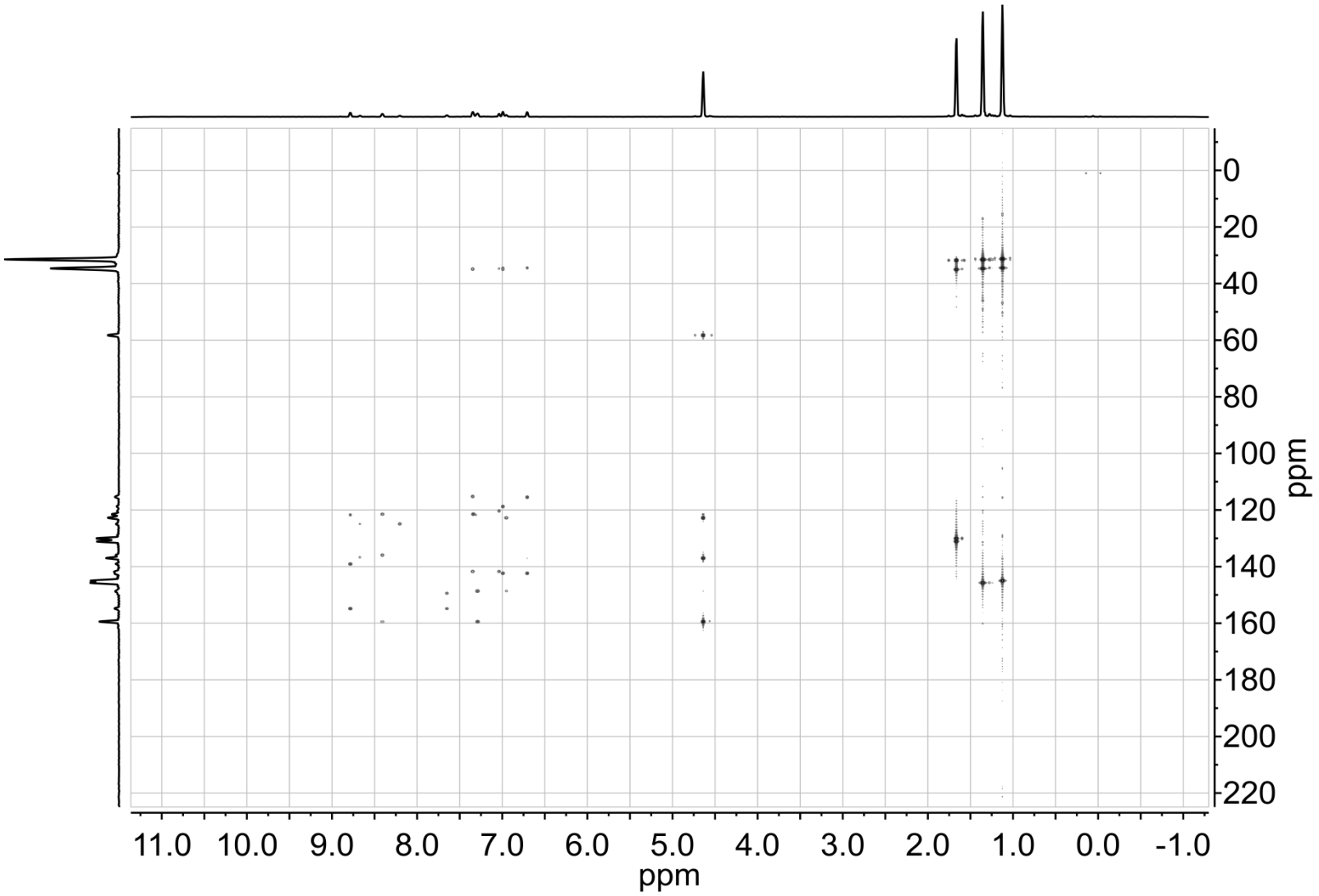

Figure S21. ^{1}H NMR (500 MHz, $C_2D_2Cl_4$) spectrum of $[Zn(iXa)(OTf)_2]$ (**6**).

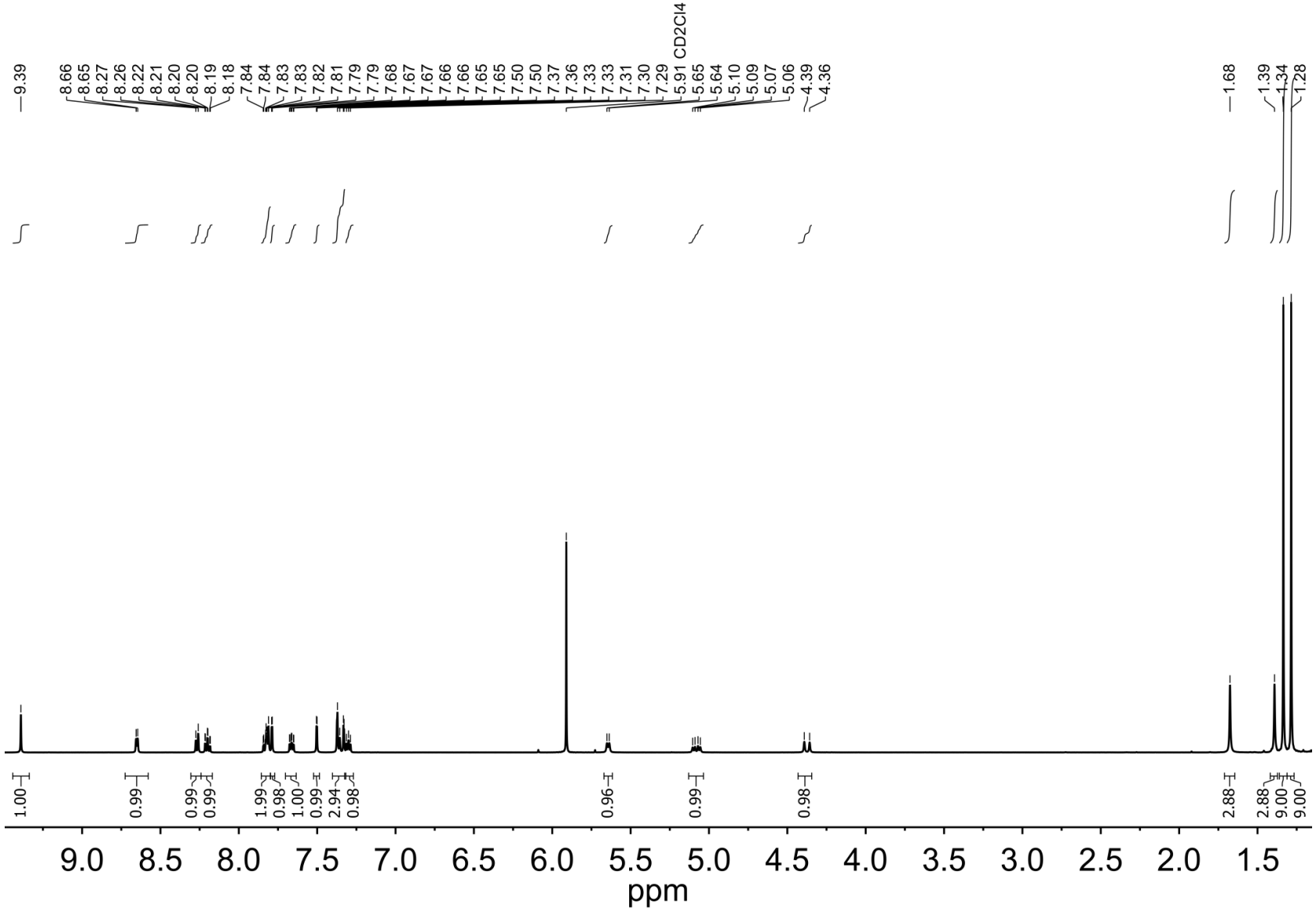

Figure S22. ^{13}C NMR (126 MHz, $C_2D_2Cl_4$) spectrum of [Zn(iXa)$(OTf)_2$] (**6**).

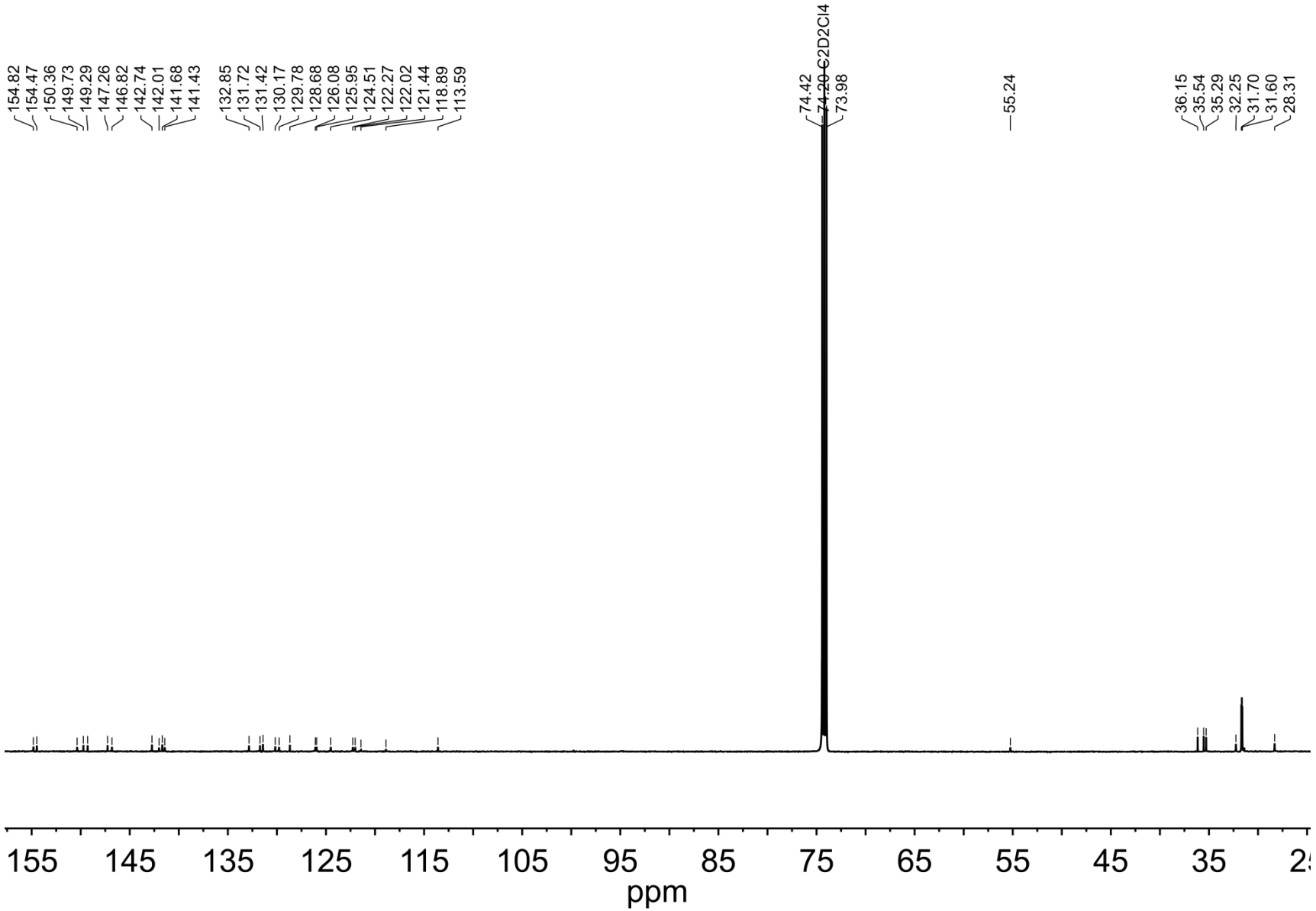

Figure S23. ^{1}H cosy-NMR spectrum (500 MHz, $C_2D_2Cl_4$) spectrum of [Zn(iXa)$(OTf)_2$] (**6**).

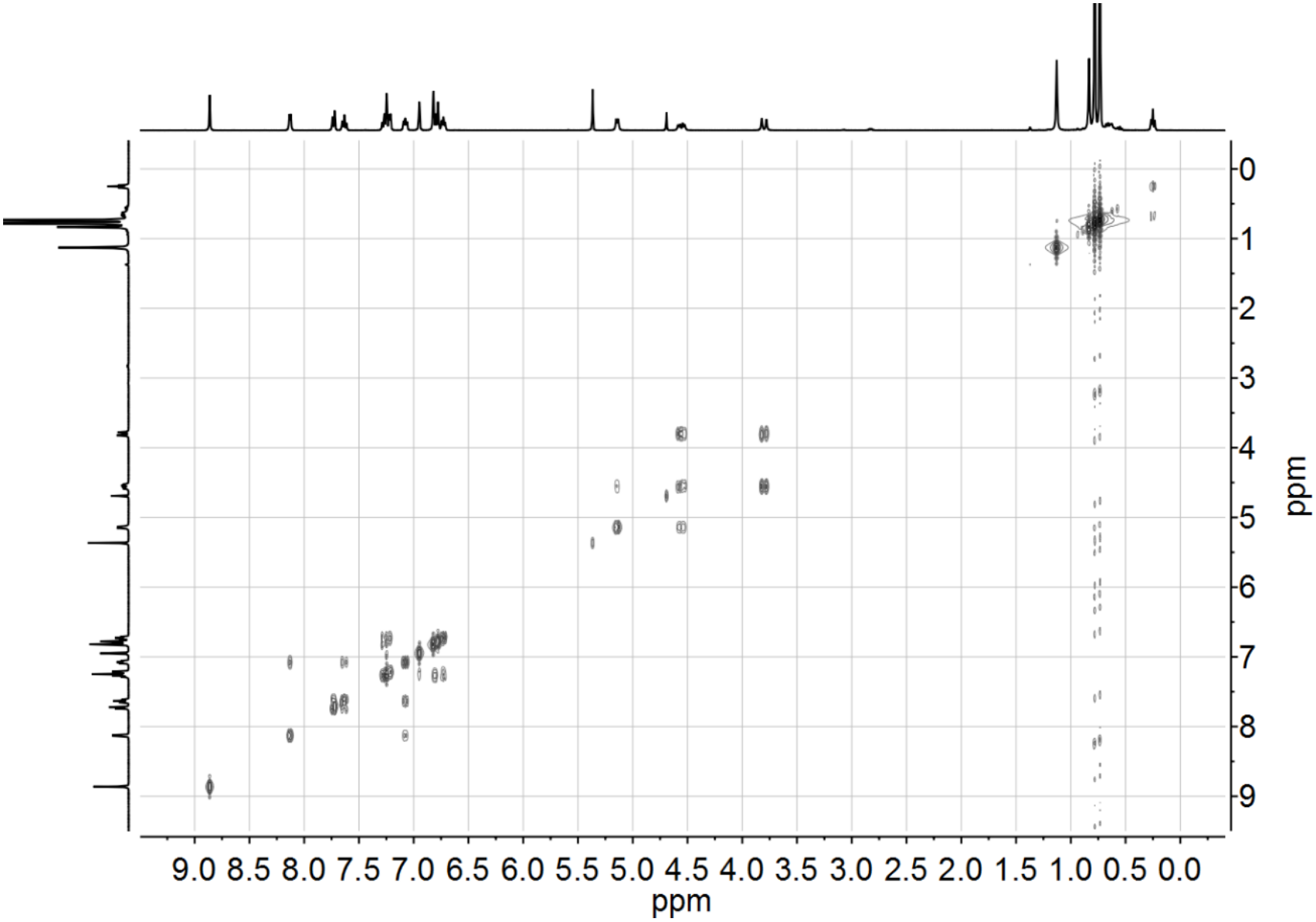

Figure S24. ^{1}H, ^{13}C HSQC-NMR spectrum (500 MHz, 126 MHz, $C_2D_2Cl_4$) spectrum of [Zn(iXa)$(OTf)_2$] (**6**).

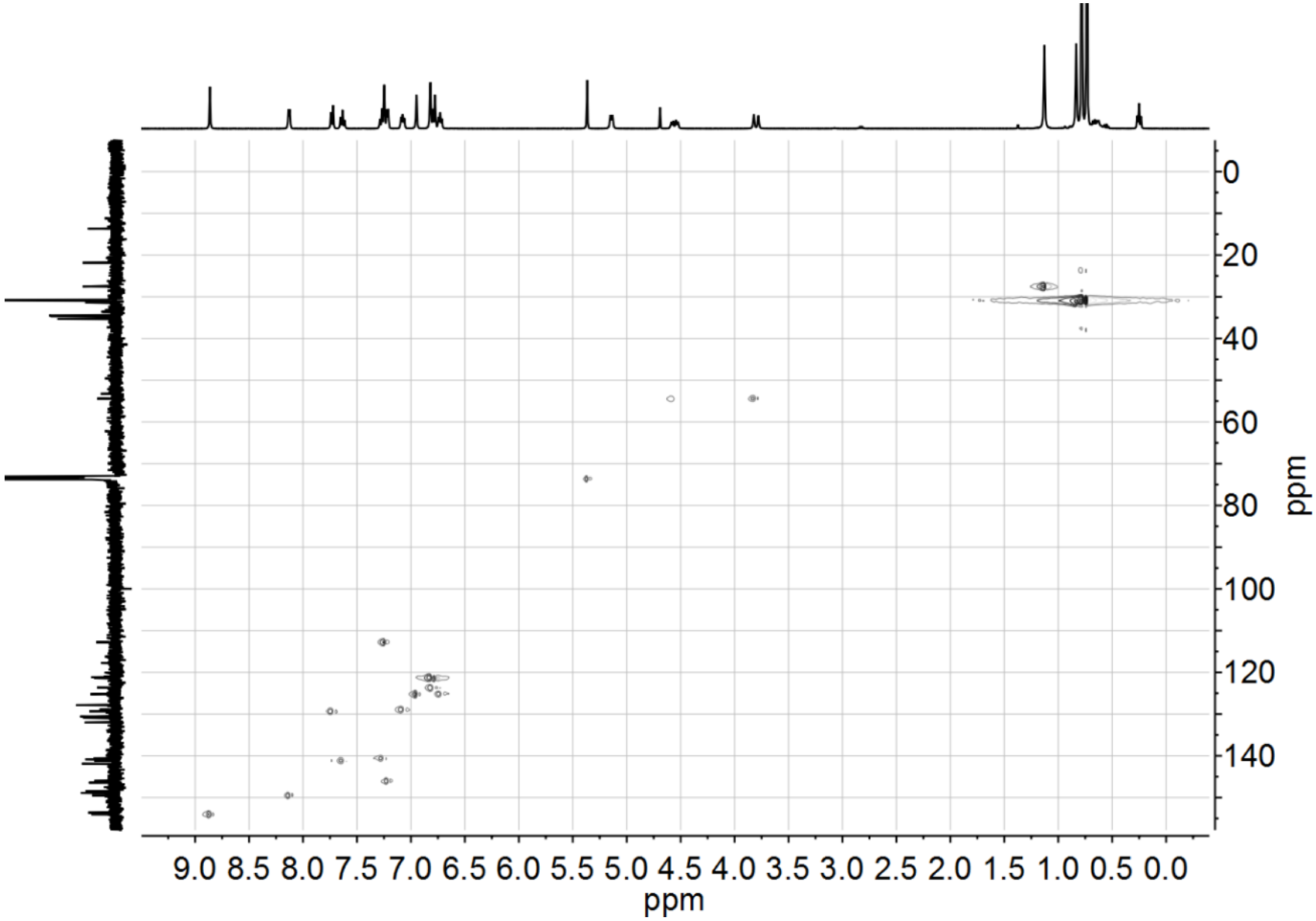

Figure S25. ^{1}H, ^{13}C HMBC-NMR spectrum (500 MHz, 126 MHz, $C_2D_2Cl_4$) spectrum of [Zn(iXa)$(OTf)_2$] (**6**).

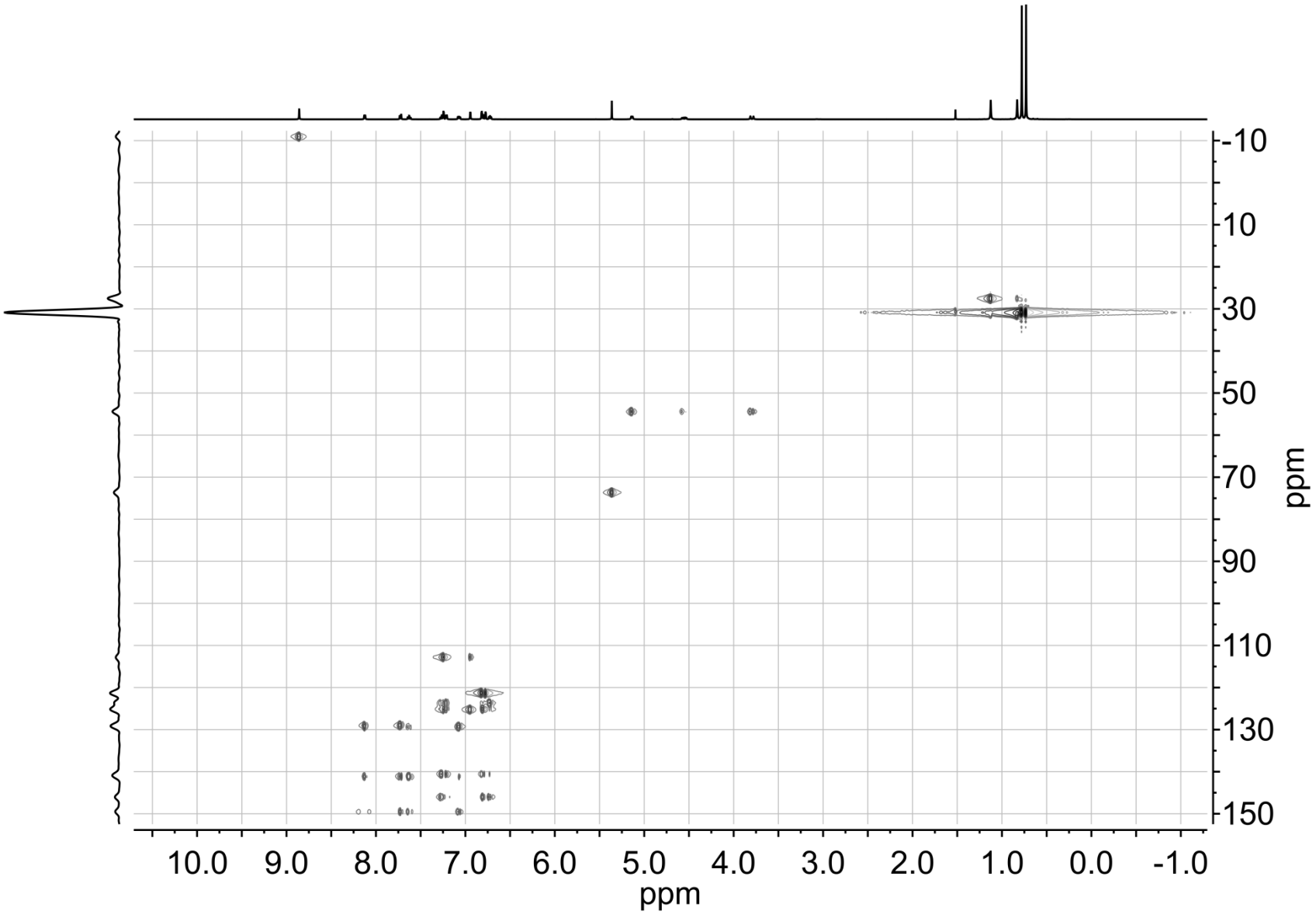

Figure S26. ^{1}H NMR (500 MHz, CD_3CN) spectrum of [Zn(iXa-2)](OTf)$_2$ (**7**).

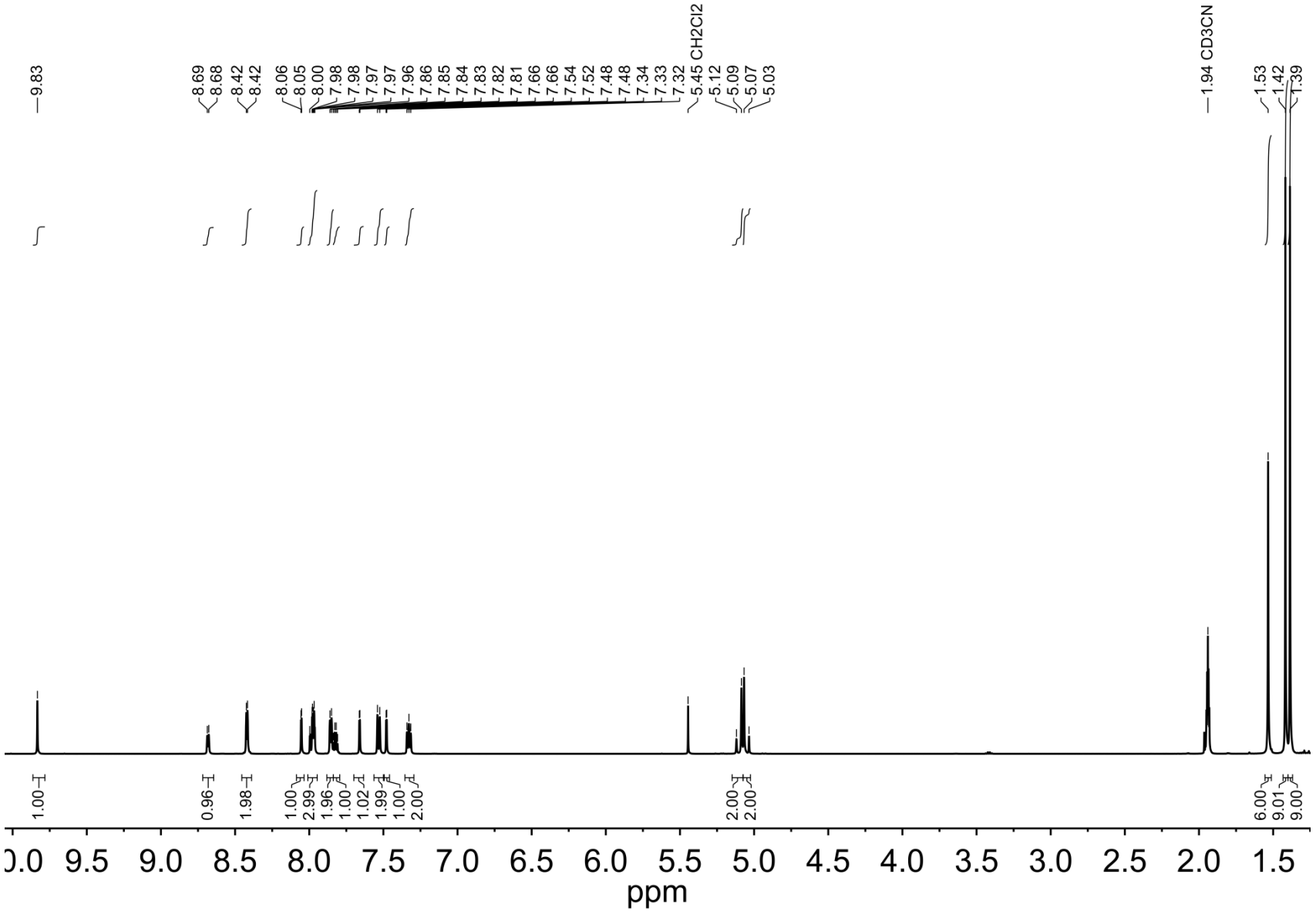

Figure S27. ^{13}C NMR (126 MHz, CD_3CN) spectrum of $[Zn(iXa\text{-}2)](OTf)_2$ (**7**).

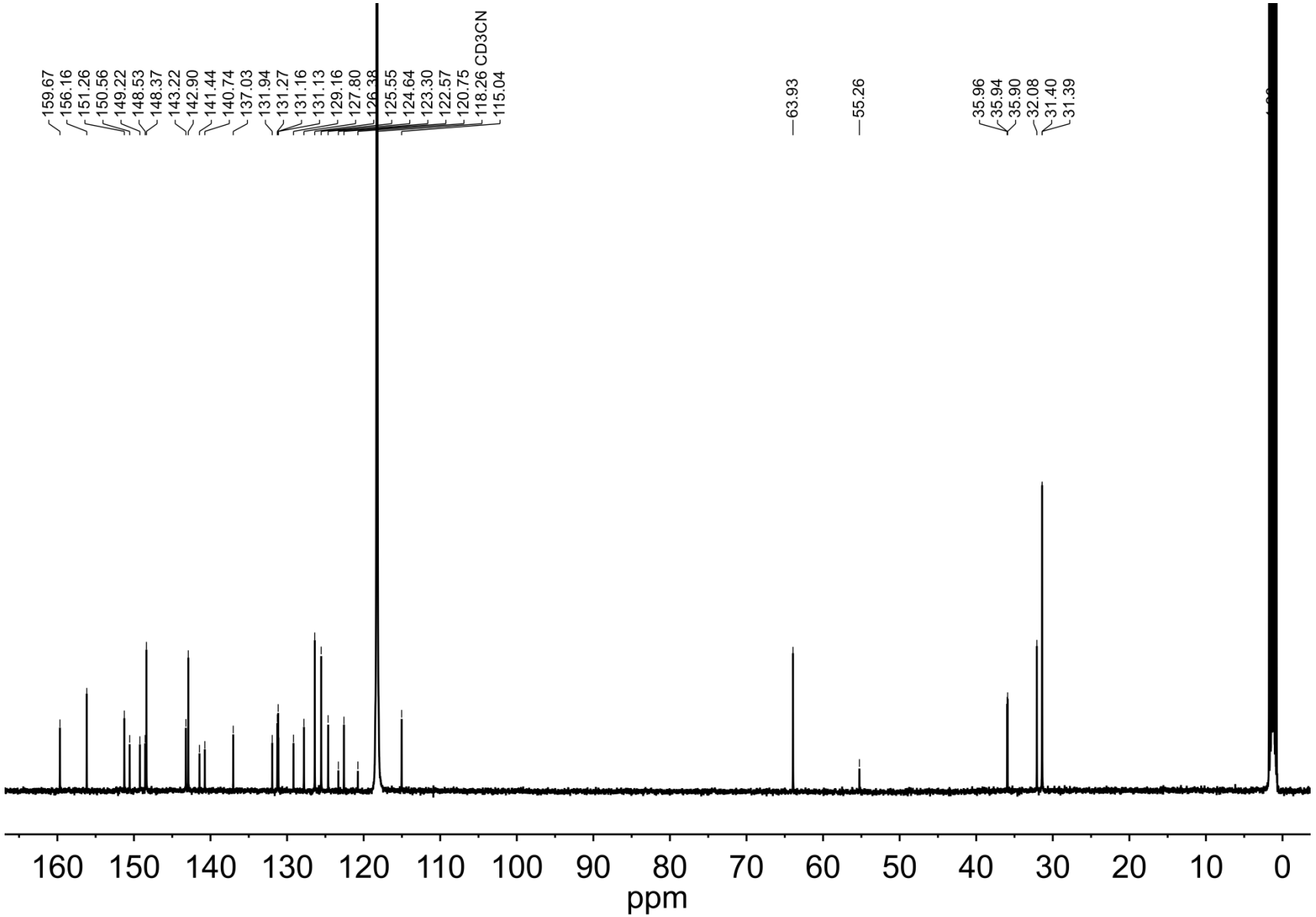

Figure S28. ^{1}H cosy-NMR spectrum (500 MHz, CD_3CN) spectrum of [Zn(iXa-2)]$(OTf)_2$ (**7**).

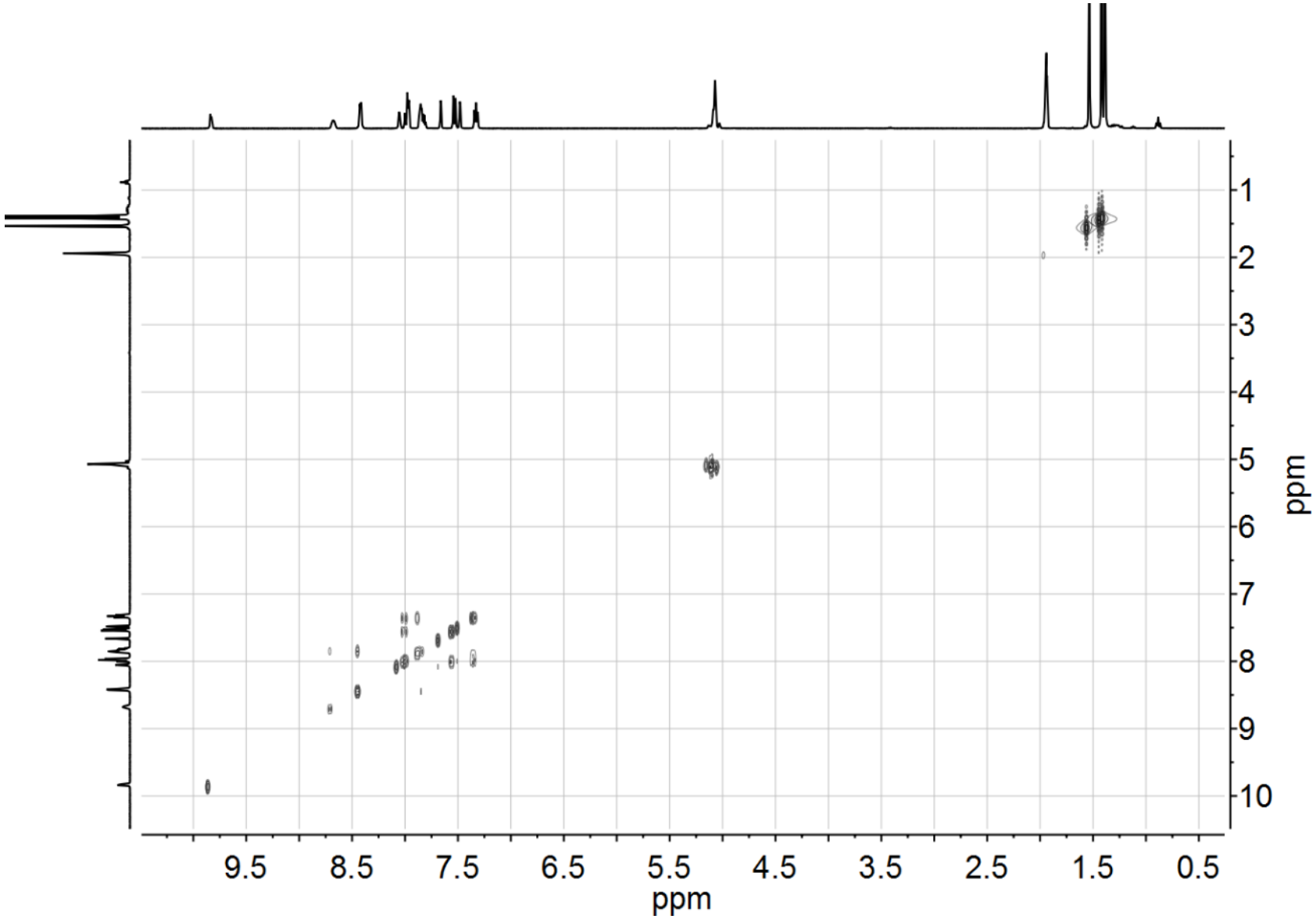

Figure S29. ^{1}H, ^{13}C HSQC-NMR spectrum (500 MHz, 126 MHz, CD_3CN) spectrum of $[Zn(iXa\text{-}2)](OTf)_2$ (**7**).

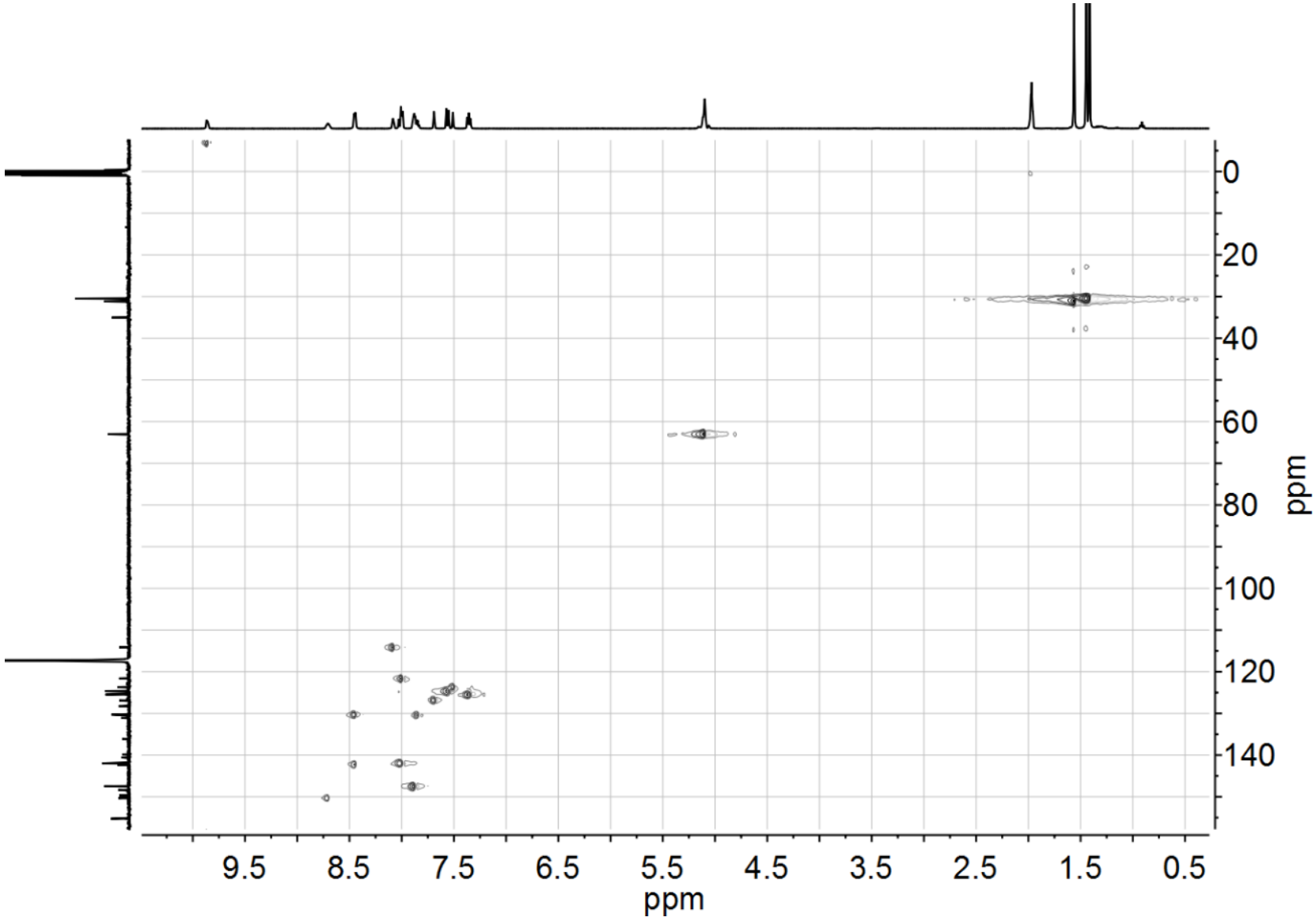

Figure S30. ^{1}H, ^{13}C HMBC-NMR spectrum (500 MHz, 126 MHz, CD_3CN) spectrum of $[Zn(iXa\text{-}2)](OTf)_2$ (**7**).

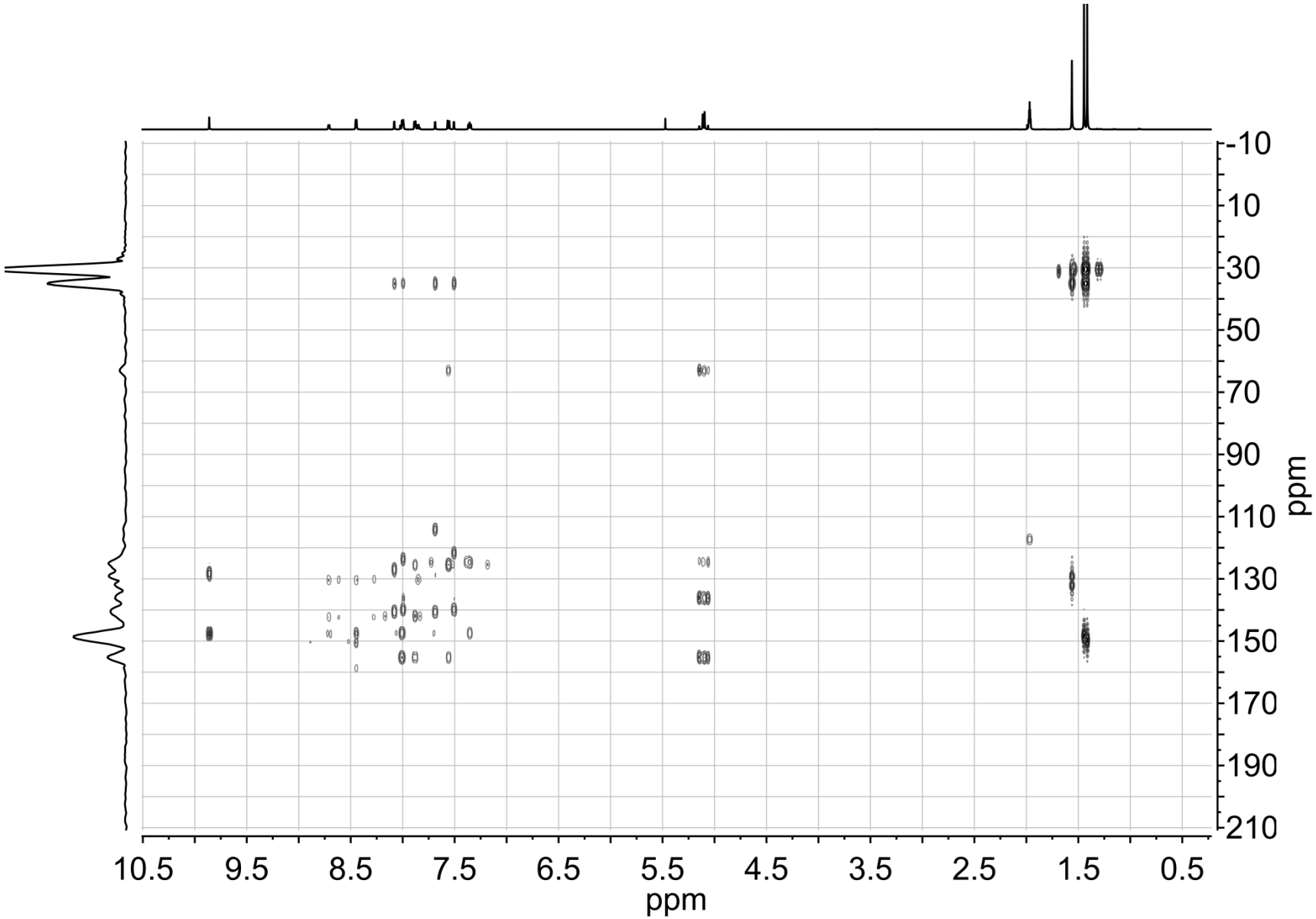

Table S1. Select Bond Distances (Å) and angles (°) for **4** - **7**.

M = Fe or Zn	**4**	**5**	**6**	**7**
M1–N1	2.244(15)	2.185(11)	2.136(2)	2.169(2)
M1–N2	2.246(14)	2.152(11)	2.216(2)	2.133(2)
M1–N3	2.335(14)	2.308(11)	2.267(2)	2.379(2)
M1–N4	2.134(14)	2.112(14)	2.096(2)	2.045(2)
M1–N5(O2)	2.152(15)	2.103(13)	2.087(2)	2.057(2)
M1–N6(O7)	2.329(16)		2.578(2)	
M1–O1	2.380(11)	2.212(10)	2.554(2)	2.273(2)
N1–M1–N2	72.71(5)	75.62(4)	76.68(7)	76.79(7)
N2–M1–O1	67.26(4)	71.58(4)	65.76(6)	71.18(6)
O1–M1–N3	68.22(4)	73.35(4)	66.73(6)	70.74(6)
N3–M1–N4	74.88(5)	76.14(5)	78.72(7)	76.83(8)
N4–M1–N5(O2)	163.74(6)	150.26(5)	165.14(7)	150.22(8)
N5(O2)–M1–N6(O7)	81.91(6)		85.05(5)	
N6(O7)–M1–N1	79.18(5)		80.60(6)	
N1–M1–N4	93.07(5)	93.89(5)	94.78(7)	99.36(8)
N5(O2)–M1–O1	84.27(5)	90.75(4)	84.27(5)	91.98(7)
N4–M1–O1	86.71(5)	92.97(5)	76.20(6)	91.48(7)
N4–M1–N6(O7)	97.02(5)		92.70(6)	
N1–M1–N5(O2)	102.60(5)	98.81(4)	99.32(6)	93.22(8)
N1–M1–N3	150.44(5)	139.37(4)	150.59(7)	141.14(7)

Figure S31. Electronic Spectra of **6** (solid line) and **7** (dashed line) in CH_3CN.

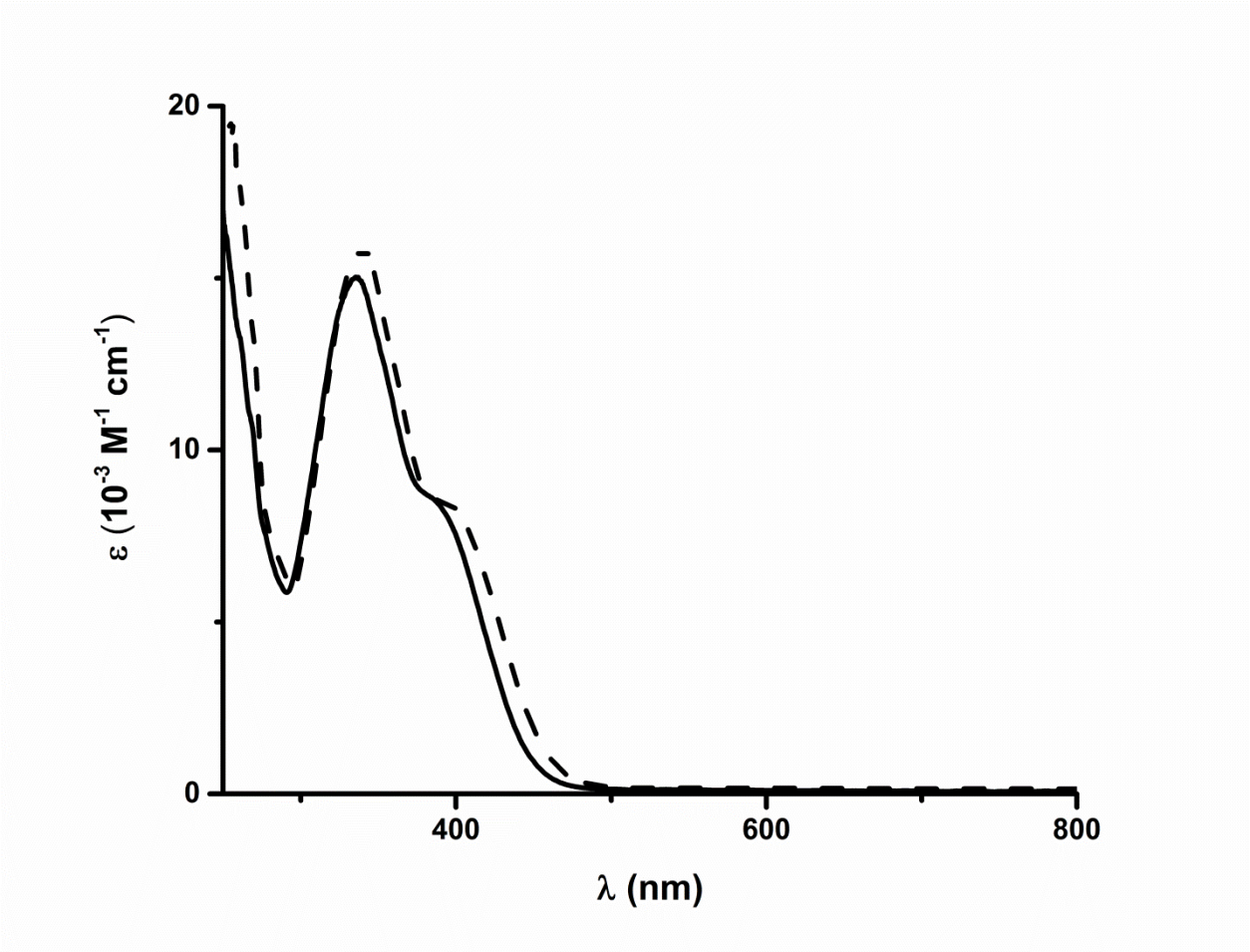

Figure S32. Full cyclic voltammograms of Top: the ligands, **iXa**- and **iXa-2**; Bottom: **4**, **5**, **6** and **7**; CH_3CN, 0.1 V s^{-1}, 0.1 M $[N(n\text{-}Bu)_4]PF_6$.

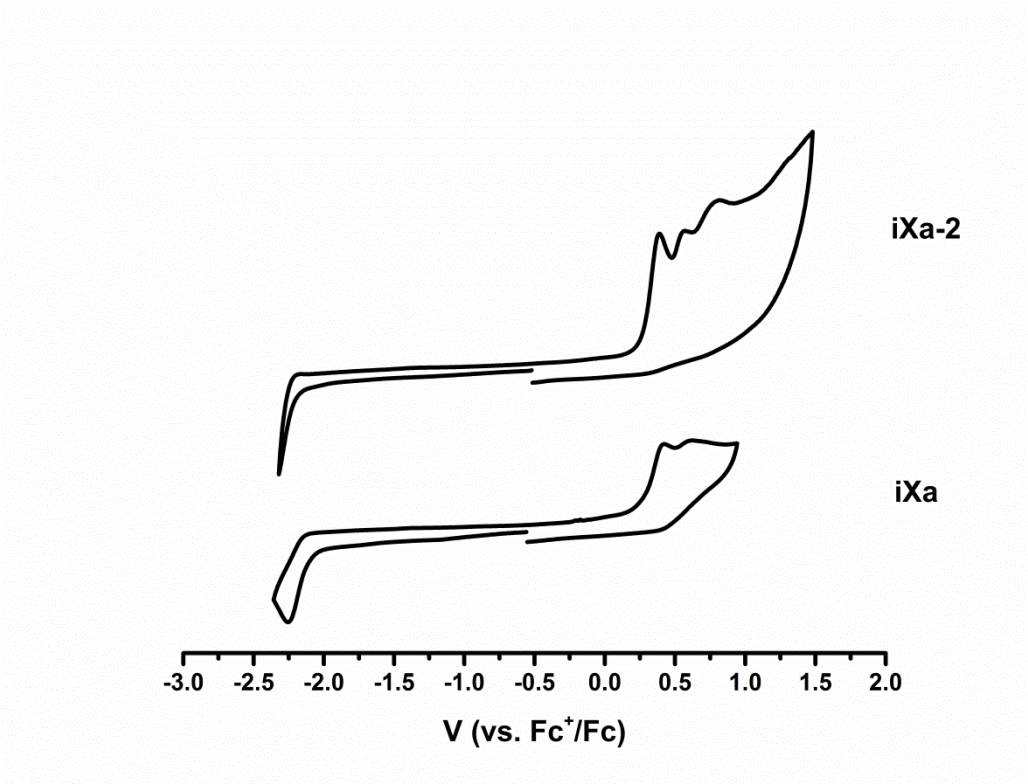

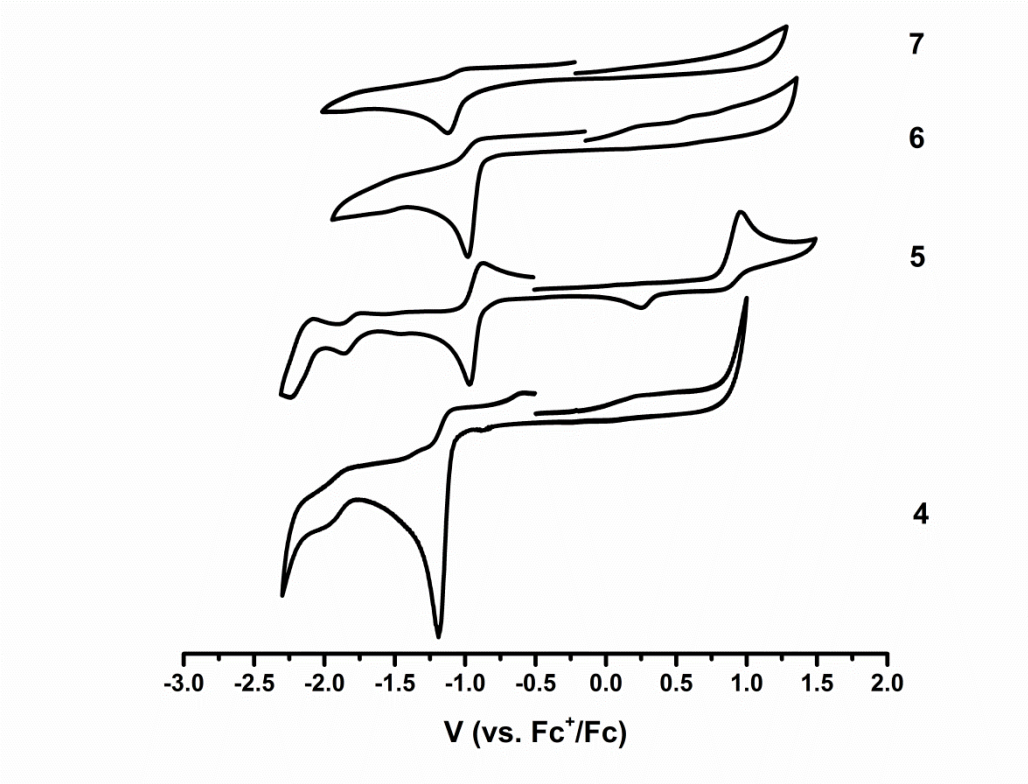

Figure S33. Temperature dependence of χ_{mol} of powdered sample **4**. Solid circles represent the experimental data; red line represents the best fit of the data (0.1 T, C = 4.52 cm^3 mol^{-1}, θ = 0.57 K).

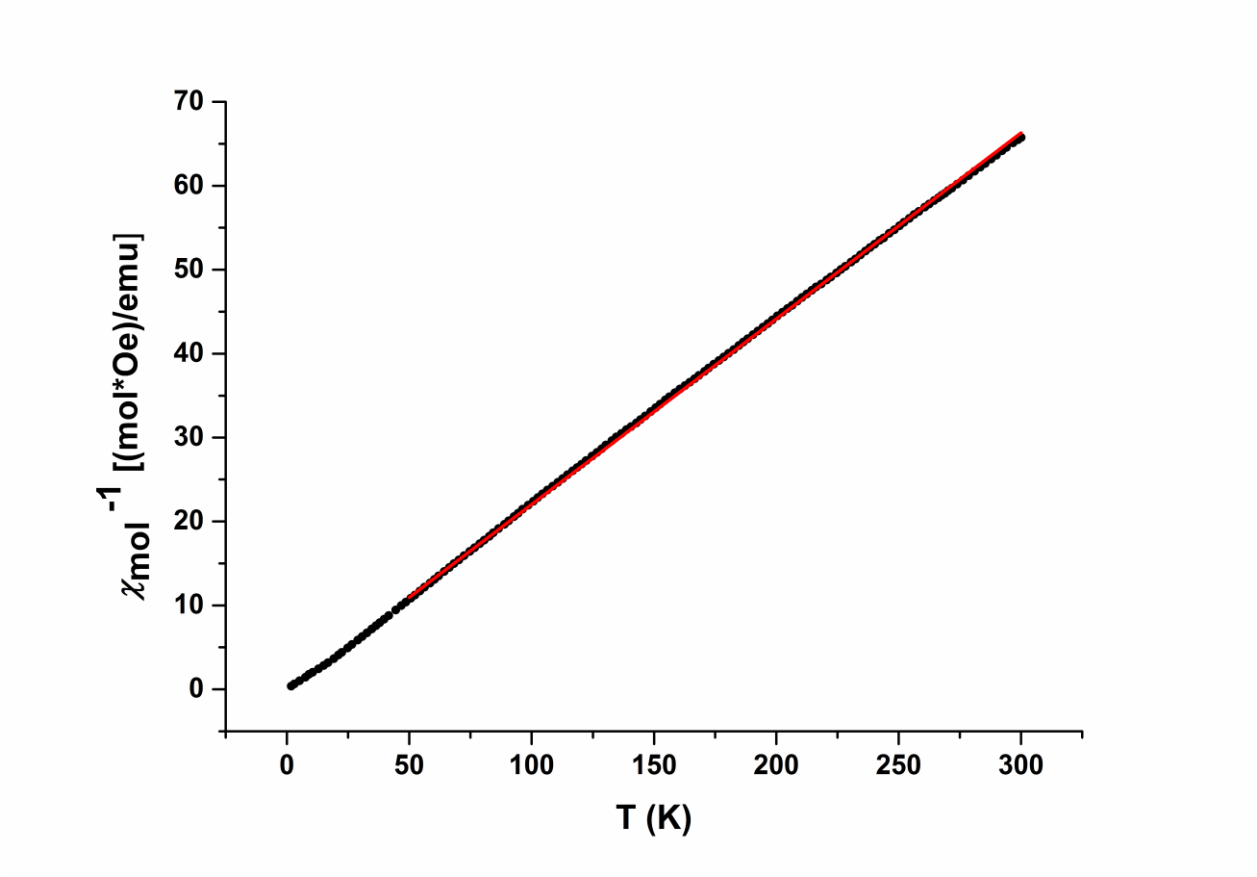

Figure S34. Temperature dependence of χ_{mol} of powdered sample **5**. Solid circles represent the experimental data; red line represents the best fit of the data (0.1 T, C = 3.80 cm^3 mol^{-1}, θ = 3.33 K).

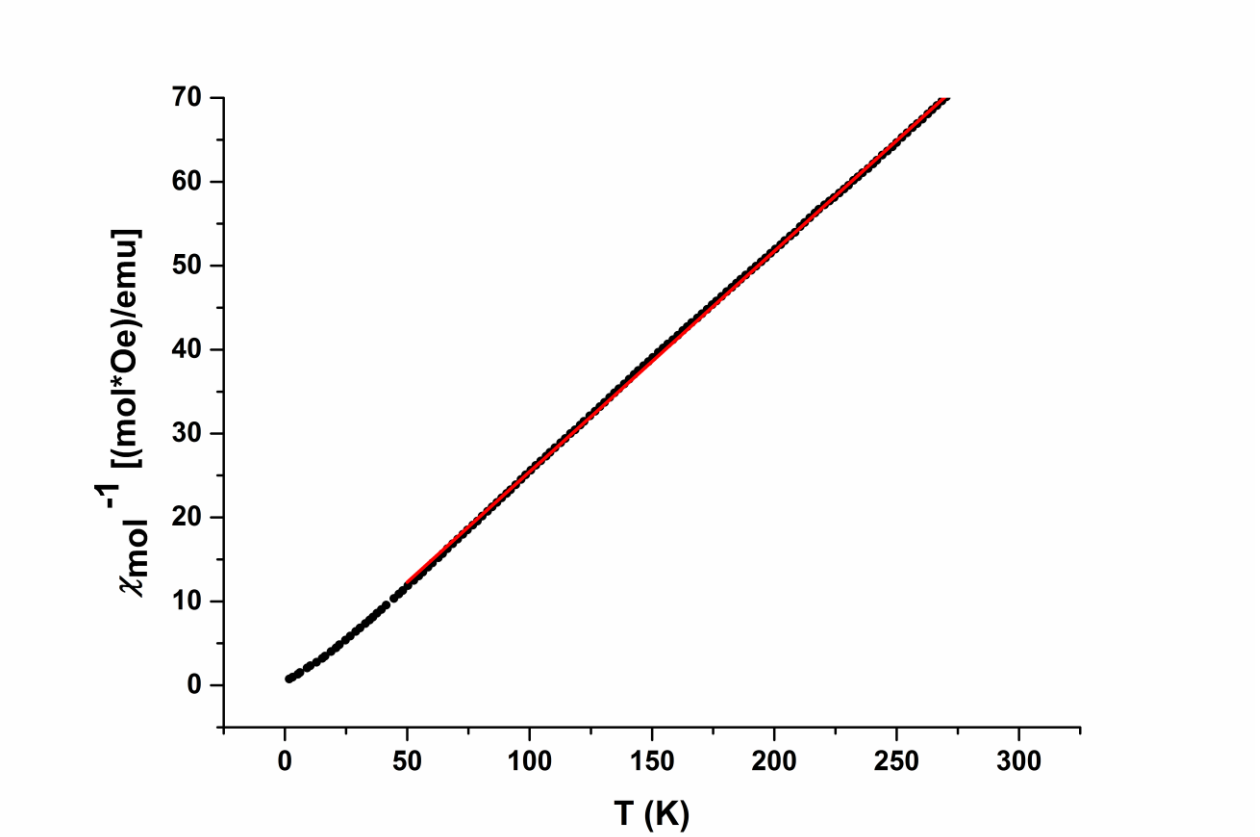

Figure S35. Temperature dependence of the magnetic moment (μ_{eff} (μ_B)) of **4** in CH_3CN (6.2 mM). Solid circles are the experimental data; red line represents the best fit of the data (1 T, solvent: CH_3CN, g_1 = 1.7, $|D_1|$ = 4.95 cm^{-1}, E/D_1 = 0, TIP = 24657 × 10^{-6} emu).

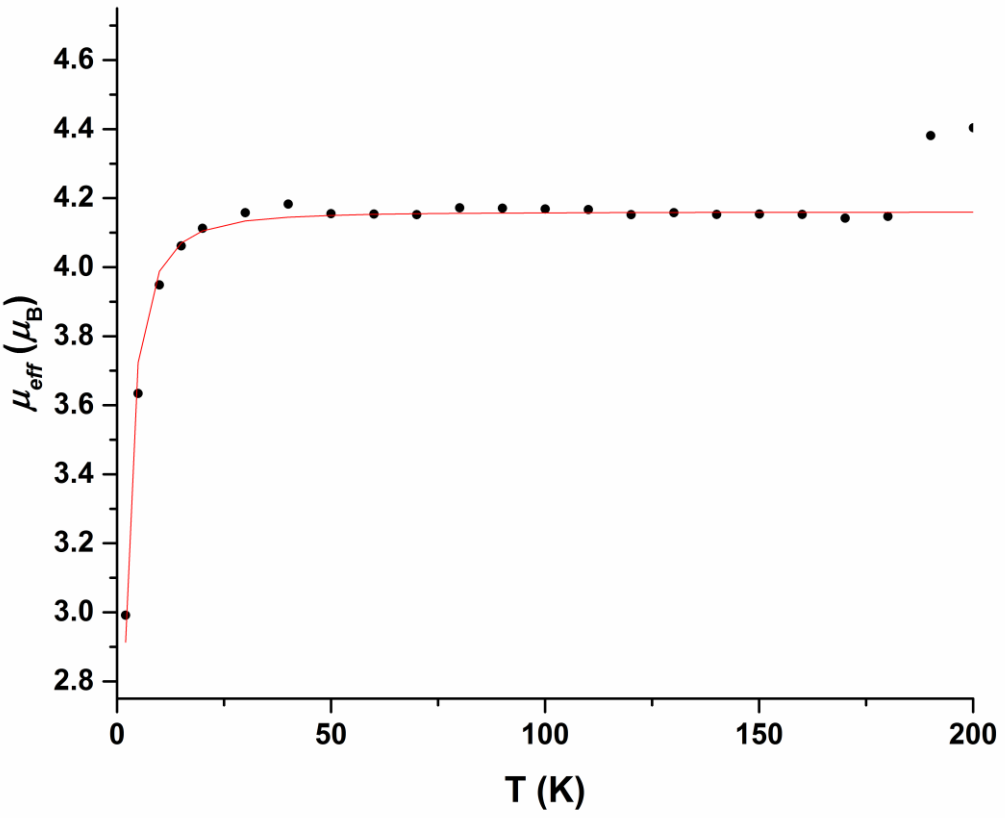

Figure S36. Temperature dependence of the magnetic moment (μ_{eff} (μ_B)) of **5** in CH_3CN (5.7 mM). Solid circles are the experimental data; red line represents the best fit of the data (Solvent: CH_3CN, g_1 = 1.5, $|D_1|$ = 5 cm^{-1}, E/D_1 = 0, TIP = 36000 × 10^{-6} emu).

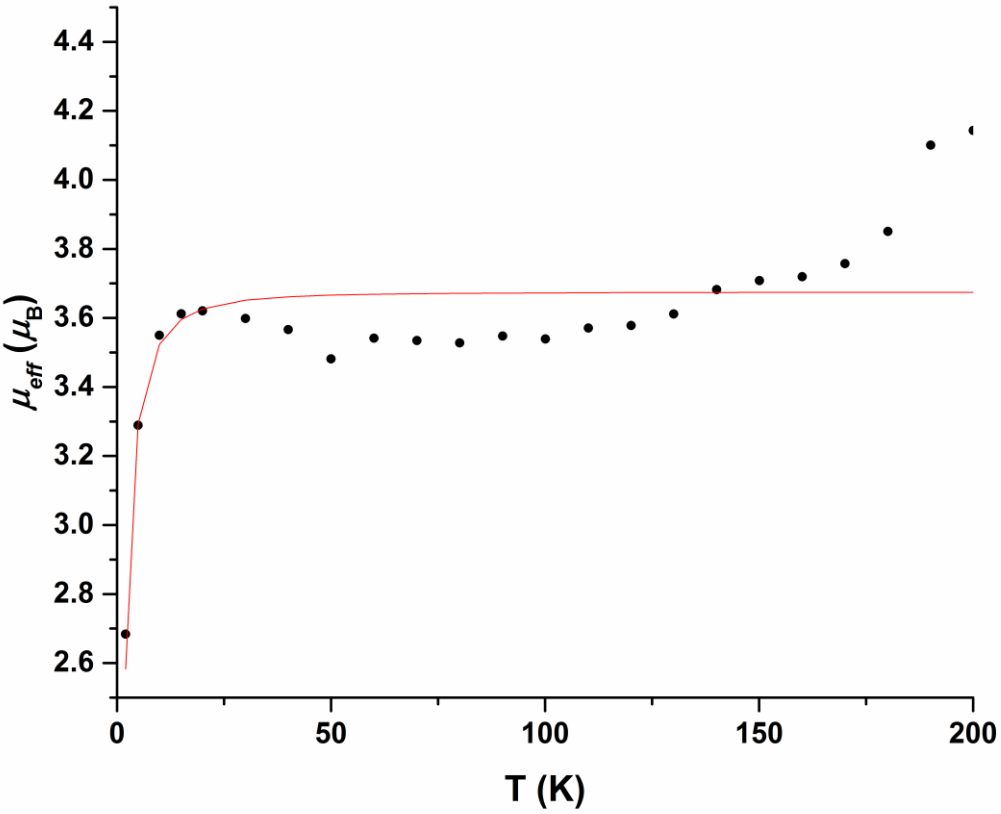

Treatment of the paramagnetic NMR data

According to eq. 1 the experimental signal shift, δ_T^{exp}, at the temperature *T* is the sum of the contact shift, δ_T^{con}, the dipolar shift, δ_T^{dip}, and the diamagnetic shift, δ^{dia}.

$$\delta_T^{\mathrm{exp}} = \delta_T^{\mathrm{con}} + \delta_T^{\mathrm{dip}} + \delta^{\mathrm{dia}} \qquad (1)$$

The contact shift, which is relevant for the signal assignment, may be determined by subtracting δ^{dia} (known from the Zn analogue) from δ_T^{exp} if the dipolar shift is small.

For estimating the dipolar shift the rhombic distortion of the compound is neglected so that eq. 2 can be used.[1]

$$\delta_T^{\mathrm{dip}} = \frac{\mu_0}{4\pi}\frac{\beta_e^2}{9k_B T}\, S(S+1)\, \frac{3\cos^2\theta - 1}{r^3}\, \left(g_\parallel^2 - g_\perp^2\right)\left[1 - \frac{7\left(g_\parallel^2 + 0.5 g_\perp^2\right)}{5\left(g_\parallel^2 - g_\perp^2\right)}\frac{D}{k_B T}\right] \qquad (2)$$

Here μ_0 is the magnetic constant, β_e is the Bohr magneton, k_B is the Boltzmann constant, *T* is the absolute temperature, *S* is the spin quantum number, *r* is the vector joining a given proton and the iron atom in the crystal, θ is the angle between *r* and the principal magnetic axis, $g_\parallel$ and $g_\perp$ are the g factors parallel and perpendicular to the main magnetic axis, respectively, and *D* is the zero-field splitting constant. Since Fe(II) *S* = 2 complexes often have short electron relaxation times and/or large *D*-values, g factors are difficult to obtain from EPR spectra. An example is $[Fe(H_2O)_6](SiF_6)$ with $g_\parallel = 2.00$, $g_\perp = 2.11$, and *D* = 12 cm^{-1} (rounded values).[2] Using the crystal structure data of **4** and **5** in Tables S3 and S2, eq. 2 yields the dipolar shifts also listed in these tables. Compared to δ_T^{para} the respective $\delta_{298}^{\mathrm{dip}}$ values are small except for protons whose paramagnetic shifts are also small (Hf and Hp of **4**). This means that the dipolar shifts can be neglected in most cases and that $\delta_T^{\mathrm{con}} \approx \delta_T^{\mathrm{exp}} - \delta^{\mathrm{dia}}$ is a reasonable approximation.

The spin densities, ρ, obtained from DFT calculations are converted into theoretical contact shifts, $\delta_T^{\mathrm{theor}}$, by applying eq. (3),[3] where it is assumed that the g-factor anisotropy is small.

$$\delta_T^{\mathrm{theor}} = \frac{a_0^3 \mu_0 g_{av}^2 \beta_e^2 (S+1)}{9k_B T}\, \rho \qquad (3)$$

All constants and variables of eq. 3 have been mentioned above except for the Bohr radius, a_0, and the average g factor, g_{av}. The calculated contact shifts are listed in Table S2 and S3. Due to the approximations used the correlation between δ_T^{para} and $\delta_T^{\mathrm{theor}}$ is not ideal. In this context, it is worth noting that the corresponding data of H_f and H_p of **4** exhibit no special behaviour although their dipolar shifts might not be negligible.

For the final signal assignment the intensities and the half widths, Δ, have been considered. The signal half width criterion assumes that the signal broadening is dominated by dipolar relaxation so that the signals become broader when the Fe···H distance decreases ($\Delta \propto r^{-6}$).[3]

Table S2. Parameters used to assign the ^{1}H NMR signals of **5**.

Label	Spin ρ [a] x 10^{-3} [a.u.]	$\delta^{exp}{}_{298}$ rel. TMS [ppm]	Integral expl.	Half-width Δ [Hz]	Fe···H distance r [Å]	Angle θ [deg]	$\delta^{dip}{}_{298}$ [ppm]	δ^{dia} from **7** [ppm]	$\delta^{para}{}_{298}$ [ppm]	$\delta^{theor}{}_{298}$ [ppm]
H_e	0.8713	224	[b]	260	3.874	105.8	1.3	9.83	214	227
H_a	0.3283	140	1.0	600	3.265	90.6	2.9	8.69	131	86
H_n	0.3135	123	2.1	950	3.564	56.1	0.1	5.06[e]	118	114
H_r	0.4385	81	2.2	720	3.093	40.1	-2.5	7.86	73	82
H_o	0.1410	54.8	2.8	75	5.029	24.2	-1.2	7.53	47.3	36.7
H_q	0.0675	51.9	2.9	60	5.091	23.1	-1.2	7.33	44.6	17.6
H_d	0.1960	50.3	1.5	55	5.034	104.1	0.6	8.42	41.9	51.1
H_b	0.1598	49.2	1.4	55	5.234	95.6	0.7	7.83	41.4	41.6
$H_{n'}$	0.0655	42	1.8	1000	3.174	53.3	-0.2	5.11[e]	37	17
H_j	0.0333	17.0	1.6	20	6.364	89.5	0.4	7.48	9.5	8.7
H_h	0.0038	15.7	1.4	30	6.346	99.6	0.4	7.66	8.0	1.0
H_l	0.0038	15.1	1.5	25	4.896	82.5	0.8	7.98	7.1	1.0
H_f	-0.0083	4.5	1.8	55	4.845	105.4	0.7	8.06	-3.6	-2.1
H_p	-0.0118	2.3	2.9	35	5.829	1.1	-1.0	8.01	-5.7	-3.1
H_g	0.0020	1.1	13.2	15	7.853	[c]	[d]	1.42	-0.3	0.1
H_k	0.0005	0.4	13.2	15	7.800	[c]	[d]	1.39	-1.0	0.5
H_i	0.0000	-0.4	8.6	20	6.451	[c]	[d]	1.53	-1.9	0.0
H_c	-0.0653	-0.9	1.3	55	5.915	100.9	0.4	8.42	-9.3	-17.0

[a] Spin per unpaired electron. [b] Not determined. [c] Not determined; see also next footnote. [d] Owing to the large distances r the dipolar shifts should be very small. For this reason the averaging of the angle θ of the methyl and *tert*-butyl groups has been abandoned. [e] Interchange of Hn and Hn' not excluded.

Table S3. Parameters used to assign the ^{1}H NMR signals of **4**.

Label	Spin ρ [a] x 10^{-3} [a.u.]	δ^{exp}_{298} rel. TMS [ppm]	Integral expl.	Half-width Δ [Hz]	Fe···H distance r [Å]	Angle θ [deg]	δ^{dip}_{298} [ppm]	δ^{dia} from **6** [ppm]	δ^{para}_{298} [ppm]	δ^{theor}_{298} [ppm]
H_e	0.6425	297	[b]	650	3.874	107.59	1.8	9.39	288	276.8
H_r	0.3125	147	1	780	3.265	39.07	-2.7	7.79	139	134.6
H_n	0.2750	130	0.8	1200	3.564	59.11	0.5	5.08	125	118.5
H_a	0.2550	96	0.9	920	3.093	79.66	2.5	8.66	87	109.8
H_d	0.1500	85	1	490	5.029	104.7	0.6	8.27	77	64.6
H_b	0.1250	63.6	1.2	380	5.091	86.7	0.7	7.66	55.9	53.8
H_o	0.1175	62.9	1.2	350	5.034	25.0	-1.1	7.36	55.5	50.6
H_q	0.0850	52.7	1.3	130	5.234	22.1	-1.2	7.30	45.4	36.6
H_j	0.0225	22.3	0.9	440	3.174	83.0	0.3	7.33	15.0	9.7
H_g	0.0010	1.2	11	15	7.929	[c]	[d]	1.34	-0.1	0.4
H_k	-0.0005	-2.5	11	10	7.734	[c]	[d]	1.29	-3.8	-0.2
H_i	0	-4.8	6.4	40	6.752	[c]	[d]	1.68	-6.4	0
$H_{i'}$	-0.0005				6.520	[c]	[d]	1.39		-0.2
H_c	-0.0275	-12.3	0.4	260	5.972	97.1	0.4	8.20	-20.5	-11.8
H_m	-0.0975	-58	[b]	2900	2.699	90.1	5.1	5.65	-64	-42.0

[a] Spin per unpaired electron. [b] Not determined. [c] Not determined; see also next footnote. [d] Owing to the large distances, *r*, the dipolar shifts should be very small. For this reason the averaging of the angle θ of the methyl and *tert*-butyl groups has been abandoned.

Figure S37. Qualitative MO diagram from DFT calculations (B3LYP) on the non-optimized, crystallographically determined structure of **4**.

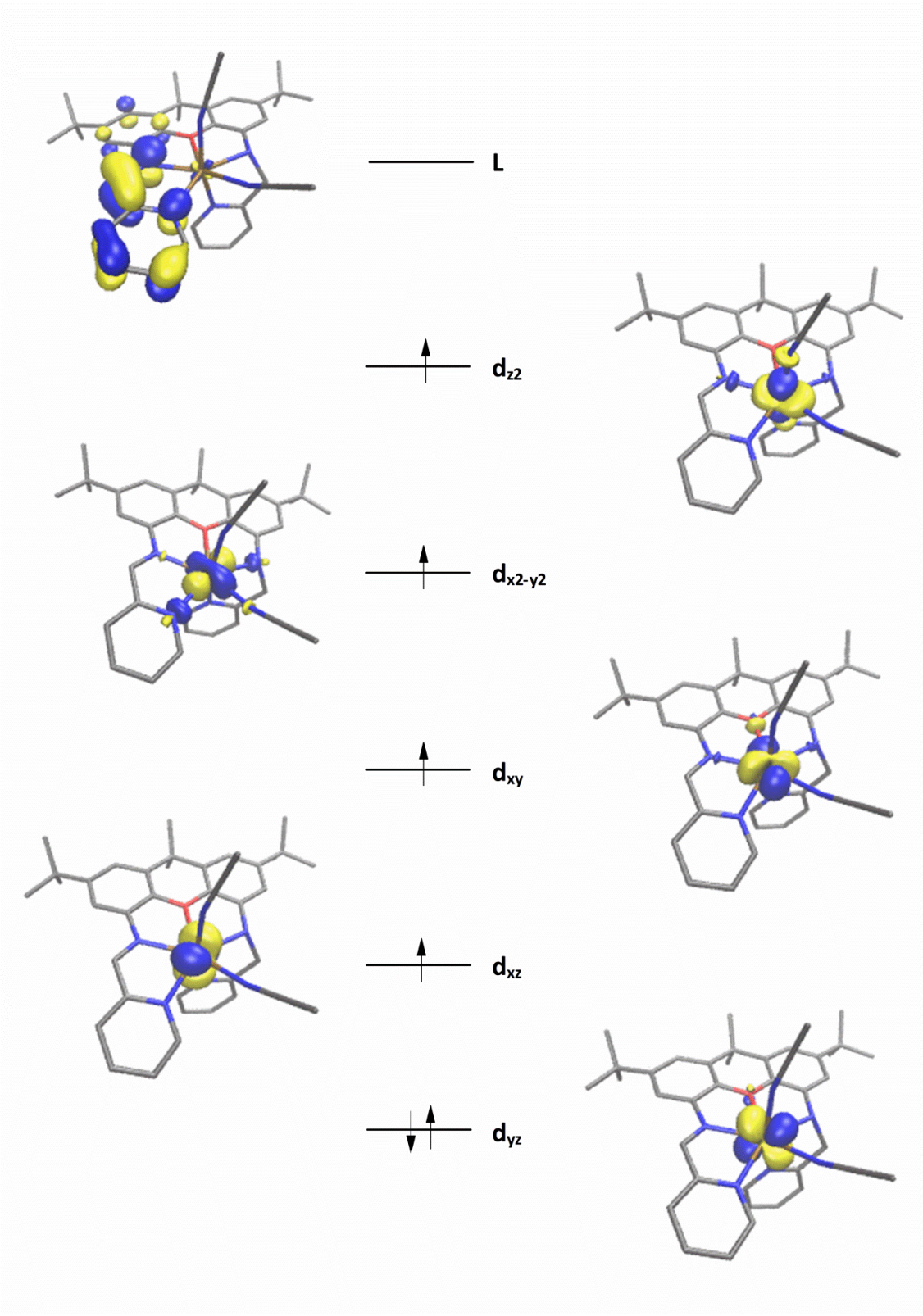

Figure S38. Qualitative MO diagram from DFT calculations (B3LYP) on the non-optimized, crystallographically determined structure of **5**.

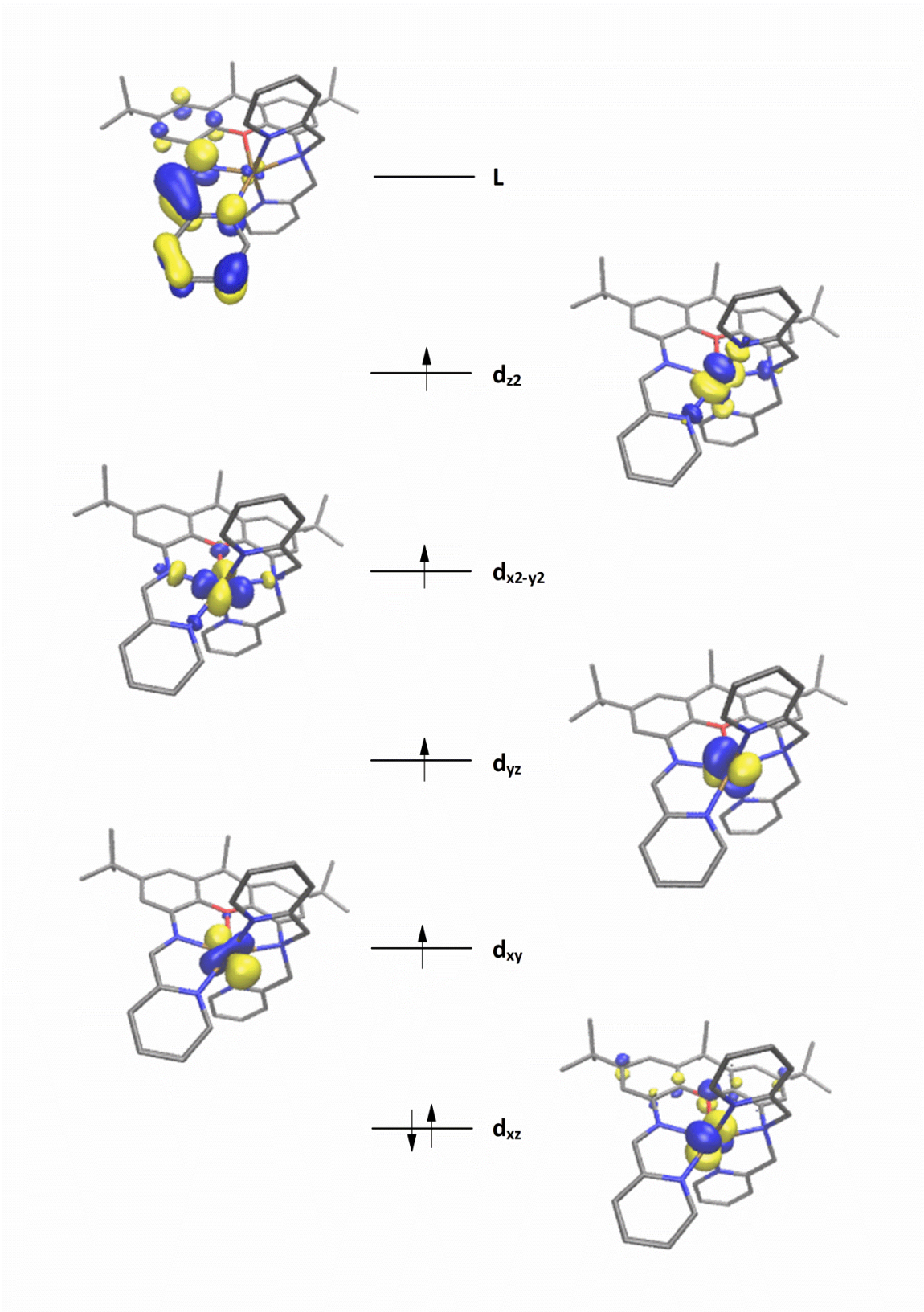

References

1. R. Acerete, N. Casan-Pastor, J. Bas-Serra and L. C. W. Baker, *J. Am. Chem. Soc.*, **1989**, *111*, 6049-6056.
2. J. Krzystek, D. Smirnov, C. Schlegel, J. van Slageren, J. Telser and A. Ozarowski, *J. Magn. Reson.*, **2011**, *213*, 158-165.
3. F. H. Köhler, in *Magnetism: Molecules to Materials*, Wiley-VCH, Weinheim, Germany, **2001**, vol. 1, ch. 12.